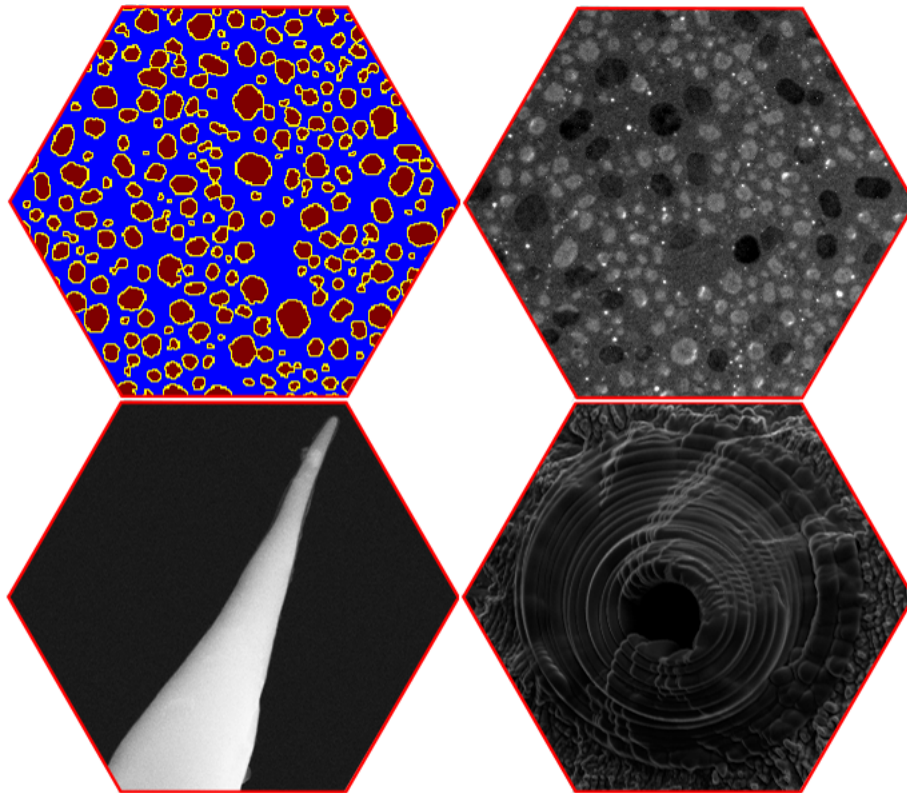




CHALMERS
UNIVERSITY OF TECHNOLOGY



Thermal *in situ* TEM experiment on nanoscale indium islands

Estimation of Electron Beam Heating Effect

Master's thesis in Applied Physics

REN QIU

MASTER'S THESIS 2017

Thermal *in situ* TEM experiment on nanoscale indium islands

Estimation of Electron Beam Heating Effect

REN QIU



CHALMERS
UNIVERSITY OF TECHNOLOGY

Department of Physics
Eva Olsson Group
CHALMERS UNIVERSITY OF TECHNOLOGY
Gothenburg, Sweden 2017

Thermal *in situ* TEM Experiment on Nanoscale Indium Islands
Estimation of Electron Beam Heating Effect

Master Thesis within the Masters Programme of Applied Physics

© REN QIU, 2017.

Supervisor: Eva Olsson, Norvik Voskanian, Lunjie Zeng, Department of Physics
Examiner: Eva Olsson, Department of Physics

Master's Thesis 2017
Department of Physics
Eva Olsson Group
Chalmers University of Technology
SE-412 96 Gothenburg
Telephone + 46(0)73-732 4883

Cover:

Top left: Indium islands segmentation by watershed algorithm based on the bright field TEM image.

Top right: Dark field image of the *in situ* melting experiment where the indium islands with bright pixels are melted and the ones with dark pixels are in solid state.

Bottom left: Nano-scale gold tip fabricated through electrochemical etching.

Bottom right: A simple Faraday cup made on the gold tip by focus ion beam (FIB) method.

Printed by Chalmers Reproservice
Gothenburg, Sweden 2017

Thermal *in situ* TEM Experiment on Nanoscale Indium Islands
Estimation of Electron Beam Heating Effect
REN QIU
Department of Physics
Chalmers University of Technology

Abstract

One of the limitations of transmission electron microscopy are the beam damaging effects that can arise from interactions between the primary high energy electron beam and the sample. The effects include radiolysis of organic and polymer materials, knock-on and sputtering damages, and beam heating induced by phonon excitation from inelastic scattering of incident electrons.

In this master thesis project, an experimental study of the local beam heating effect is carried out using electron thermal microscopy technique based on transmission electron microscope (TEM) dark field imaging. *In situ* heating experiments with different beam settings in the TEM are performed on nanoscale indium islands deposited on top of 50 nm thick silicon nitride membrane through metal evaporation. The specimen is heated by a TEM heating holder and the amount of beam heating is quantified by evaluating the change in melting point of the indium island.

For easier data analysis, image processing is done to identify the indium islands in the bright and dark field images. First, OTSU thresholding and Watershed algorithm are used on the bright field image to recognize the indium islands. Dark field images are then rigidly aligned with respect to the bright field image so that all indium islands are identified through the whole melting process. The melting temperature of each indium island of interest is then determined from the change in contrast in the dark field image at the transition temperature from solid to liquid state.

The acceleration voltage, the illumination area and the beam current are the three main parameters of the incident electron beam influencing the amount of induced beam heating in a sample. Effect of the acceleration voltage at 120 and 200 kV is compared. The electron beam illuminating area on the sample is estimated using a standard TEM grating sample. The beam currents are measured using the TEM fluorescent screen, which is independently calibrated as part of this work. A custom made Faraday cup is produced on a gold tip using a focused ion beam (FIB). The Faraday cup is mounted in a *Nanofactory* holder and the beam current is measured with a picoammeter. The calibrated conversion coefficient for the beam current is then determined by comparing the current values measured by the Faraday cup and the fluorescence screen.

The melting temperature of the indium islands is used as a reference point to quantify the heating effect of the electron beam. The beam heating is investigated as a function of electron beam current and acceleration voltage by measuring the change

of the indium island melting temperature registered on the external heating control unit. Based on the observations, a method to quantify the local electron beam heating in TEM is proposed. This is important for quantitative data evaluation of *in situ* thermal TEM experiments.

Keywords: TEM, beam heating effect, dark field imaging, indium, image analysis.

Acknowledgements

First, I would like to thank my supervisors professor Eva Olsson, doctor Novik Voskanian and doctor Lunjie Zeng for helping me in the project. I would also like to thank Anders Kvist and Stefan Gustafsson for the kind help and suggestions on my experiments. Finally, I want to say thanks to my beloved family for supporting my master study in Sweden.

Ren Qiu, Gothenburg, July 2017



Contents

List of Figures	xiii
List of Tables	xix
1 Introduction	1
1.1 Radiolysis	1
1.2 Knock-on & Sputtering Damaging	2
1.3 Beam Heating Effect	2
1.4 Scope of Master Thesis	2
2 Electron Microscopy	3
2.1 Scanning Electron Microscope	3
2.2 Focused Ion Beam Microscope	3
2.3 Transmission Electron Microscope	4
2.3.1 TEM Construction	4
2.3.2 TEM Imaging Modes	5
3 Sample Preparation	9
3.1 Indium Islands	9
3.2 Sharp Gold Tip	10
3.3 Faraday Cup	12
4 Thermal Experiment	15
4.1 Electron Thermal Microscopy	15
4.2 Heating Holder	15
4.3 Heating Process	16
4.4 Electron Beam Calibration	18
5 Image Analysis	21
5.1 OTSU Threshold	21
5.2 Watershed Segmentation	22
5.3 Image Alignment	23
6 Results	25
6.1 Gold Tip	25
6.1.1 One - step Etching	25
6.1.2 Two - step Etching	26

6.2	Homemade Faraday Cup	28
6.3	Beam Current Calibration	29
6.4	Island Identification	30
6.5	Electron Beam Heating	32
7	Conclusion & Future Plan	39
A	Matlab Code	I
A.1	Main File	I
A.2	Image Alignment	III
A.3	Image Segmentation	IV
A.4	Island Analysis	V
A.5	Melting Analysis	VII
A.6	Melting Sequence Analysis	IX
A.7	Melting Data	X
A.8	Image Display	XIII

List of Figures

2.1	Schematics of TEM configuration [9]. TEM is composed of the illumination system, imaging forming system and the projection and image recording system.	5
2.2	Schematic ray diagram illustration of TEM imaging modes. (A) Bright field imaging mode where only the forward electron beam is allowed through the objective aperture. (B) Dark field imaging mode operates while one diffracted beam is selected by the objective aperture. (C) Centered dark field imaging mode where objective aperture is placed on-axis and diffracted electron beam gets selected to give image contrast by tilting the incident electron beam [2].	6
3.1	Electron beam transparent thick silicon nitride membrane with thickness of 50 nm lying on top of a 200 μm thick frame of silicon with a 250 μm \times 250 μm transparent window for electron beam's passing through. The sample was brought from obtained from <i>Norcada</i> [11]. (a) is the top view optical micrograph. (b) is the schematic diagram of the cross section where the light blue represents the silicon nitride film and the dark blue is the silicon frame.	9
3.2	Nanoscale indium islands deposited on the silicon nitride thin film. (a) SEM image of indium islands deposited on the silicon nitride membrane. (b) Schematic diagram illustrating the indium islands deposited on the 50 nm thick silicon nitride membrane. Silicon nitride membrane is drawn in light blue. The indium islands are drawn with the indium core in yellow and the oxidized shell in green.	10

- 3.3 Schematic diagrams of the experiment setup and principles of the electrochemical etching process. (a) Schematic configuration of experiment setup for gold tip preparation based on electrochemical etching. The anode gold wire is immersed into the etchant solution based on concentrated hydrochloric acid (37%) together with the surrounding cathode providing a uniform electric field that is cylindrical isotropic under external bias provided by the DC power supply. (b) is the basic process of one-step etching method where gold wire is immersed into the etchant with a constant depth L and a tip apex is formed with dropping of lower part caused by narrowing of gold wire at the taper. (c) shows two-step etching process where gold wire is immersed into the etchant with L_1 at first to be etched for a time period as t^* , which is followed by an increment of immersion depth to be L_2 and finally tip is formed by the breaking at the first taper region. 11
- 3.4 A schematics of a TEM Faraday cup [2] where a metallic chamber is covered by a small aperture for electron beam to pass through. Secondary electrons and back scattered electrons generated in the metallic chamber are blocked by the aperture diaphragm made of platinum. An insulated wire connects the chamber to a picoammeter which measures the value of incident beam current with high accuracy. 12
- 3.5 Dimensions of the Faraday cup fabrication by FIB - SEM. (a) represents the area on the gold tip with diameter of $100\ \mu\text{m}$ that is chosen for the ion milling. A blind hole with diameter of $30\ \mu\text{m}$ and $60\ \mu\text{m}$ deep is drilled by ion beam, as illustrated in (b). (c) is the illustration of platinum deposition patterns where platinum is deposited as rings on top of each other step by step that gives an open hole for primary electrons with $5\ \mu\text{m}$ in diameter. (e) SEM image of the Faraday cup on the gold tip. Arrows are the marks that help to find the cup regions marked by green box. 13
- 4.1 Dark field imaging on indium solid to liquid phase transitions [7]. (a) shows the bright field image of indium islands under room temperature. (b) is a composite diffraction pattern of the indium islands in solid and liquid phases [7]. The white circle is the position of select area aperture where diffracted beam is collected for the dark field imaging. (c) is the diffraction pattern of solid indium islands [7]. (d) is the diffraction pattern of molten indium islands [7]. (e) and (f) are the dark field images of solid and liquid islands respectively where a sudden contrast change in the island pixels corresponds to the liquid-solid phase transition. Scale bar is $200\ \text{nm}$ 16
- 4.2 TEM holder for the *in situ* heating experiment. (a) is the front side of the heating holder where the frame rod, heating wire made of tungsten and the heating oven made of platinum are marked as (A), (B) and (C) respectively. (b) is the back side of the holder where (D) is a pair of thermal couple for temperature measurement. 17

4.3	Heating process of the <i>in situ</i> experiment after the determination of beam tilting angle of the centered dark field imaging. The specimen is heated up from room temperature to 60°C and stabilized for 15 minutes. The melting region of indium islands is found to be between 100°C and 130°C following this heating process depending on the island size and the electron beam condition.	17
4.4	Illumination area calibration using the standard cross grating sample from <i>Agar Scientific</i> [26]. (a) shows that the size of one grid is 463 nm. (b) is an image of the illuminated area projected on the fluorescent screen indicating a diameter of 18.29 μm by counting the number of periodic grids. The image is taken by phone camera.	18
4.5	Illustration of the beam current measurement. (a) is the side view where the electron beam is first focused at the tip front. The eucentric height is lowered by 50 μm to align the height of the beam spot with respect to that of the Faraday cup aperture. (b) is the top view. Three marks A, B and C are made by ion milling at the edge of the tip to help adjust the orientation of the tip and find the cup aperture. (c) shows the SEM image from the top view.	18
5.1	OTSU thresholding result of the bright field image. (a) TEM bright field image in gray scale. (b) Binary image obtained from OTSU threshold. (c) Pixel intensity histogram of the bright field image where the optimal threshold is calculated as 0.5608 from OTSU algorithm. Pixels with intensity above this threshold is classified as silicon nitride and the ones with intensity lower than this threshold are categorized into that belonging to the indium islands.	22
5.2	Example of the watershed segmentation. (a) Initial binary image obtained from bright field image through OTSU threshold. (b) Distance transform of (a). (c) Three dimensional plot of distance transform where two catchment basins represent the corresponding islands. (d) Result of watershed segmentation where pixels in yellow represent the edge and the ones in brown are that of indium islands. Pixels in blue represent the background.	23
5.3	Illustration of the dark field image alignment. (a) and (c) is the dark field image under 115°C and 120°C. A tiny bright feature of the indium oxide nano particle is marked out by the red circle whose positions in (a) and (c) are shown in sub-figure (b) and (d) respectively. The red arrow in (d) means that the dark field image (c) should be rigidly shifted towards left by one pixel to align well with respect to image (a).	24

-
- 6.1 Images and corresponding etching current variations of tips made from one-step etching method by gold wire with $250\ \mu\text{m}$ diameter. The etching solution is a mixture of concentrated hydrochloric acid (37%) and ethanol(99.7%) with 1:1 volume ratio. DC voltage of 2.4 V is applied between the anode and cathode sides. (a) shows a typical gold tip made by a *EL561R* power supply with immersion depth of 1 mm. (b) shows the image of a gold tip produced by immersion depth of 1 mm under DC bias 2.4 V provided by a commercial potentiostat *Gamry Interface 1000* under *Physical Electrochemistry* mode. (c) shows a image of tip made with same parameters as (b) but only increasing the immersion depth from 1 mm into 2 mm. Plot (d) and (e) give periodic variations of etching current corresponding to the tips shown as (b) and (c) respectively. Etching current after breaking of meniscus is shown in the reduce window. (f) gives the typical value of background current of the etching system with open circuit. 27
- 6.2 Gold tip prepared through two-step etching method. (a) Tip region is formed at taper 1 marked by the green rectangular box. The yellow box shows the taper 2 formed during the second step etching. (b) shows the corresponding tip at taper 1, which is extremely smooth over a large spatial scale but with the sharpness sacrificed. (c) Etching current variation of two step etching. Gold wire has diameter of $250\ \mu\text{m}$. Commercial potentiostat *Gamry Interface 1000* provides 2.4 V DC voltage by *Physical Electrochemistry* mode. In the first step, immersion depth is 1 mm and etching time (t^*) is chosen to be 390 s. In the second step, immersion depth is increased to be 2 mm and taper 1 breaks after another 95 s. 28
- 6.3 SEM images of the Faraday cup made by FIB - SEM method. In sub-diagram (a), three rectangles are milled to help determine the orientation of the gold tip in the TEM. (b) shows the structure of the Faraday cup where the aperture is made by platinum deposition. 29
- 6.4 Example of the electron beam current calibration by the homemade Faraday cup and the picoammeter in a *Nanofactory* TEM holder. Random noise is eliminated by Fourier filtering. 29
- 6.5 Calibration of beam current of the Tecnai T20 TEM. The linear coefficients between the current value given by the fluorescent screen of the TEM and the value measured by the homemade Faraday cup are 1.2716, 1.1983 and 1.1499 for the acceleration voltages to be 200 kV, 120 kV and 80 kV respectively. 30
- 6.6 Indium island identification result from the OTSU threshoding and watershed segmentation. (a) TEM bright field image. (b) Island identification after applying the OTSU threshoding and watershed segmentation on the bright field image (a). 31
- 6.7 Melting process recorded through TEM dark field imaging. The melting process happens from $110\ ^\circ\text{C}$ to $130\ ^\circ\text{C}$. The indium islands melted at $110\ ^\circ\text{C}$ and $115\ ^\circ\text{C}$ are marked by green circles. 31

6.8	Melting process shown by binary images. The same melting process is shown by the dark field images in Figure 6.7.	32
6.9	Holder temperature at melting point as a function of primary beam current at 120 kV and 200 kV acceleration voltages. The island diameter is 100 nm. The error bars are estimated to be 5°C which is half of the interval between heating steps.	34
6.10	Holder temperature at melting point as a function of primary beam current density at 200 kV acceleration voltage. The island diameter is 100 nm.	34
6.11	Holder temperature at melting point as a function of primary beam power. The island diameter is 100 nm. A linear relationship is found between the beam heating and the electron beam power.	36
6.12	Holder temperature at melting point as a function of primary beam current. The island diameter is 50 nm.	36
6.13	Holder temperature at melting point as a function of primary beam current. The island diameter is 100 nm.	37
6.14	Holder temperature at melting as a function of primary beam current. The island diameter is 200 nm.	37

List of Tables

6.1	Parameters of the <i>in situ</i> melting experiments.	33
-----	---	----

1

Introduction

In transmission electron microscopy, electrons in the primary beam are accelerated to high energies by electric field corresponding to short wavelengths to achieve the sub-nanometer (nm) spatial resolution. The Coulomb interactions between the incident electrons and the specimen result in electron scatterings which are categorized into elastic and inelastic scatterings according to the energy loss of primary electrons. Elastic scattering with no energy dissipation of primary electrons arises from the electrostatic interaction between primary electrons and the stationary atomic nuclei of the sample which gives rise to the diffraction pattern and the phase contrast [1]. It is the interactions between incident electrons, the electron cloud and the lattice phonons that cause the inelastic scattering [1]. In the inelastic scattering, energy of the incident electrons is dissipated through physical processes like the electron-phonon interaction, emission of characteristic X-rays, generation of secondary electrons, plasmon excitation, and *etc* [2]. Fine structures of the electron energy loss spectroscopy (EELS) map the typical inelastic scattering interactions except for the phonon excitation. Regardless of the type of the scattering, the accelerated high energy electrons will lead to damaging effects of the sample inevitably. Typically, the electron beam damage can be classified as radiolysis, knock-on and sputtering, and specimen heating effects [1,2]. Even though, hydrocarbon contamination caused by the beam can be eliminated by plasma cleaning, resulting in a temporary, most beam effects permanently modify the sample under investigation. It is important to evaluate and quantify these beam effects to perform TEM experiment on samples that are sensitive to high energy electrons.

1.1 Radiolysis

In radiolysis damage, chemical bonds break during the ionization process when incoming high-energy electrons interact inelastically with the corresponding bonding electrons of the sample. This permanent damage mostly happens in polymer or organic materials where the carbon chains are broken together with formation of non-bonding electrons and radicals. To reduce the radiolysis damage, electron dose should be kept below the critical values for specific materials [1,3]. Lowering sample temperature is another approach to reduce the radiation damage [3], which can be implemented by the cryo TEM technique. Jiang, *et al* studied the radiolysis effect of inorganic materials by EELS pointing out that the dose and dose rate of electron beam influence the bond breaking [4].

1.2 Knock-on & Sputtering Damaging

The knock-on damage happens due to the electrostatic interaction between incoming electrons and the atomic nucleus causing a displacement of specimen atoms together with the corresponding point defect, which usually happens near the grain boundary [3]. Sputtering process also arises from the scattering between incident electrons and the specimen nuclei, which happens when specimen atom is ejected away from the sample surfaces [2]. Both the knock-on and sputtering effects appear only if the incident beam energy is higher than the displacement activation energy of specific atoms, which explains why they mostly happen around the defect or at the surface.

1.3 Beam Heating Effect

Electron beam heating effect comes from the phonon excitation during the inelastic scattering process. In reference [5], electron beam heating of metallic sample in scanning electron microscope (SEM) is proportional to the power of incident beam. Hobbs predicted the typical temperature increase induced by transmitted electron beam for various materials by calculation indicating more heating effect for materials with low thermal conductivity [6]. Egerton *et al* calculated beam heating in TEM based on the equilibrium of heat generation by inelastic scattering the heat dissipation through thermal conduction and radiation [1]. In their model, temperature rise is notably proportional to the incident beam current. Nevertheless, they indicate that the illumination area has negligible contribution to the beam heating. However, TEM beam heating effect is not clearly investigated experimentally. Main factors influencing the specimen heating like acceleration voltage and beam current need to be studied.

1.4 Scope of Master Thesis

In this master thesis project, experiments are performed with electron thermal microscopy (EThM) method, proposed firstly by Brintlinger *et al*. It enables measurement of local temperatures with sub-100 nm spatial resolution for the *in situ* heating TEM experiment [7]. In EThM, nanoscale indium islands are deposited on top of a silicon nitride thin film. A liquid to solid phase transition of indium island during the *in situ* heating process is recognized through TEM dark field imaging, which indicates a local temperature to be the melting point of the corresponding indium island. Baloch *et al* studied the remote Joule heating of carbon nanotube [8] by EThM. More details regarding EThM will be discussed in chapter 4.

The heating experiment is carried out in a LaB6 thermionic gun Tecnai T20 TEM with acceleration voltages of 200 kV and 120 kV. An approach to precisely measure the primary beam current is also discussed in details in chapter 4. The amount of beam heating is estimated from the change of melting temperature of nanoscale indium islands.

2

Electron Microscopy

The main part of this thesis is concerned with electron microscopy, which, as a powerful technique for materials characterization, provides the possibility for combining high resolution imaging and analysis of crystallographic and chemical information. In this thesis work, different electron microscopes are used, such as SEM (scanning electron microscope), TEM and FIB-SEM, for sample characterization and *in situ* heating experiment. Basic working principles of these electron microscopes are discussed in this chapter.

2.1 Scanning Electron Microscope

In SEM, focused electron probe is scanned through the interested area of the sample. Signals generated from the specimen surface include secondary electron (SE2), back scattered electron (BSE) and characteristic x-ray, and *etc.* SE2 signal emitted from a few top layers of atoms of the sample surface gives spatial resolution as high as 1 nm with information regarding surface morphology of the specimen. The spatial resolution depends on the integral effect from specific material composition, electron probe size and the acceleration voltages. BSE signal from a larger area of the interaction volume provides image contrast depending on the atomic number of element. Characteristic x-ray is excited when incident electron undergoes inelastic scattering and the energy dissipated excites photons from a larger area of the interaction volume. It enables us to get information about the chemical composition of the interested area.

In this thesis, a LEO Ultra 55 SEM equipped with a field emission gun (FEG) is used for sample characterizations of the gold tips. These tips, made by electrochemical etching are used for the fabrication of the Faraday cup, which is discussed in details in chapter 3.

2.2 Focused Ion Beam Microscope

FIB microscope is usually used for sample preparation by ion milling. A liquid metal ion source is heated to evaporate heavy ions, usually gallium ions, flowing to a connected extremely sharp tungsten tip forming a small point source. A strong electric field is then applied to the tungsten needle to extract the gallium ions out from the tip generating a beam of heavy ions. With the ion beam, FIB microscope is able to fulfill imaging, milling and metal deposition with designed pattern at interested

area. Analogous to the SE2, secondary ions can be detected to construct a surface image with morphological information. In the milling mode, primary gallium ions emitted from the tungsten needle tip with high kinetic energies are focused on the interested sample surface area to bombard target atoms away from the bulk. A FIB instrument equipped with a gas injection system implements the deposition of platinum with desired thickness guided by the primary gallium ion beam scanning in the patterned area.

In this project, a FEI Versa3D FIB-SEM microscope is used for the fabrication of a Faraday cup on the gold tip. First, ion milling was used to fabricate a hole in the gold tip. Next, platinum deposition was used to form an aperture around the hole, partially covering the cavity. More details about the Faraday cup fabrication are discussed in chapter 3 and chapter 6.

2.3 Transmission Electron Microscope

2.3.1 TEM Construction

TEM consists of the illumination system, the image forming system, the projection and image recording system. Electrons generated from the illumination system hit the sample and get scattered. The scattered electrons are then collected to form the image and diffraction pattern by the image forming system. The Final image is recorded on an electron fluorescent screen or a CCD (Charge Couple Device) camera in the projection and image recording system, as illustrated in Figure 2.1.

In the illumination system, thermionic or field emission gun works as the electron source where the emitted electrons are accelerated by an electrostatic field. The primary electrons from the gun are collected by a strong condenser lens to form a demagnified image of the source tip. This demagnified image is projected by another weaker condenser lens onto the specimen giving a specific illumination area. Condenser apertures with various sizes are implemented inside to make the beam less divergent.

As the most critical component of TEM, the image forming system mainly consists of objective lens and its corresponding apertures. Objective lens placed beneath the specimen projects the transmitted electrons to form a diffraction pattern on the back focal plane and a sample image on the image plane. Selected area diffraction can be realized by inserting the selected area aperture into the image plane of the objective aperture. Bright and dark field images are taken by selecting desired diffracted beams within the back focal plane of the objective lens through the objective aperture.

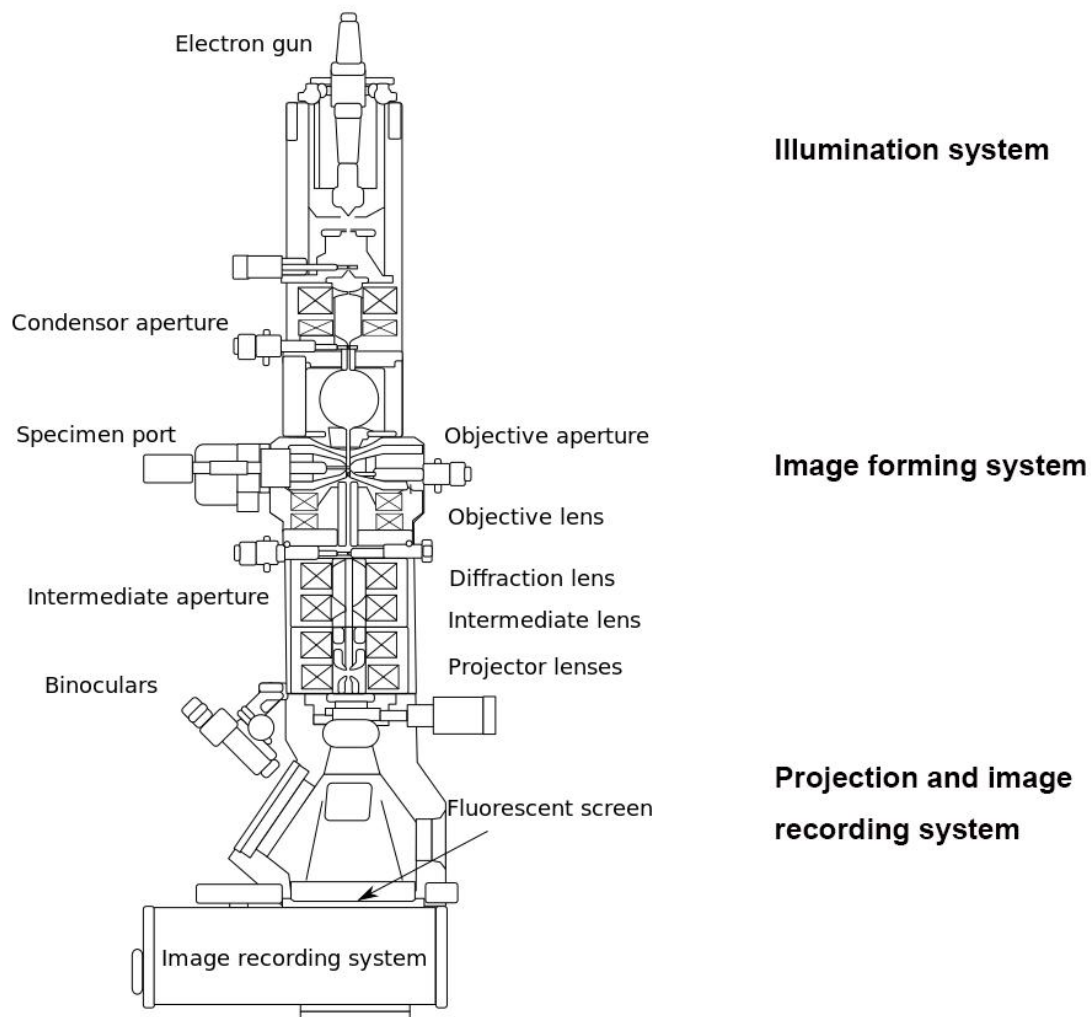


Figure 2.1: Schematics of TEM configuration [9]. TEM is composed of the illumination system, imaging forming system and the projection and image recording system.

Image or diffraction pattern formed by the objective lens is collected by the image projection and recording system. This system is composed of several lenses, including intermediate lens, projection lens, diffraction lens, an electron fluorescent screen, and a CCD camera.

In this project, the *in situ* heating experiment is performed by a FEI Tecnai T20 TEM equipped with a LaB6 thermionic gun. Bright and dark field imaging modes are performed through the heating process to recognize the indium islands and record their melting.

2.3.2 TEM Imaging Modes

There are three modes in parallel beam TEM imaging where the image contrast is determined by the size and position of the objective aperture inserted in the back

focal plane of the objective lens, as schematically illustrated in Figure 2.2. In the bright field imaging mode, the non-deflected electron beam, which is the centered diffraction spot in the diffraction pattern, is selected by the objective aperture at the back focal plane of the objective lens, as seen in Figure 2.2 (A). In the dark field imaging, as shown in Figure 2.2 (B), specific diffracted electron beam passes through the objective aperture giving rise to the image contrast of corresponding crystallographic orientation. In the centered dark field imaging mode, as illustrated in Figure 2.2 (C), objective aperture is always aligned with the optical axis within the back focal plane selecting diffracted spot through tilting of the incident electron beam.

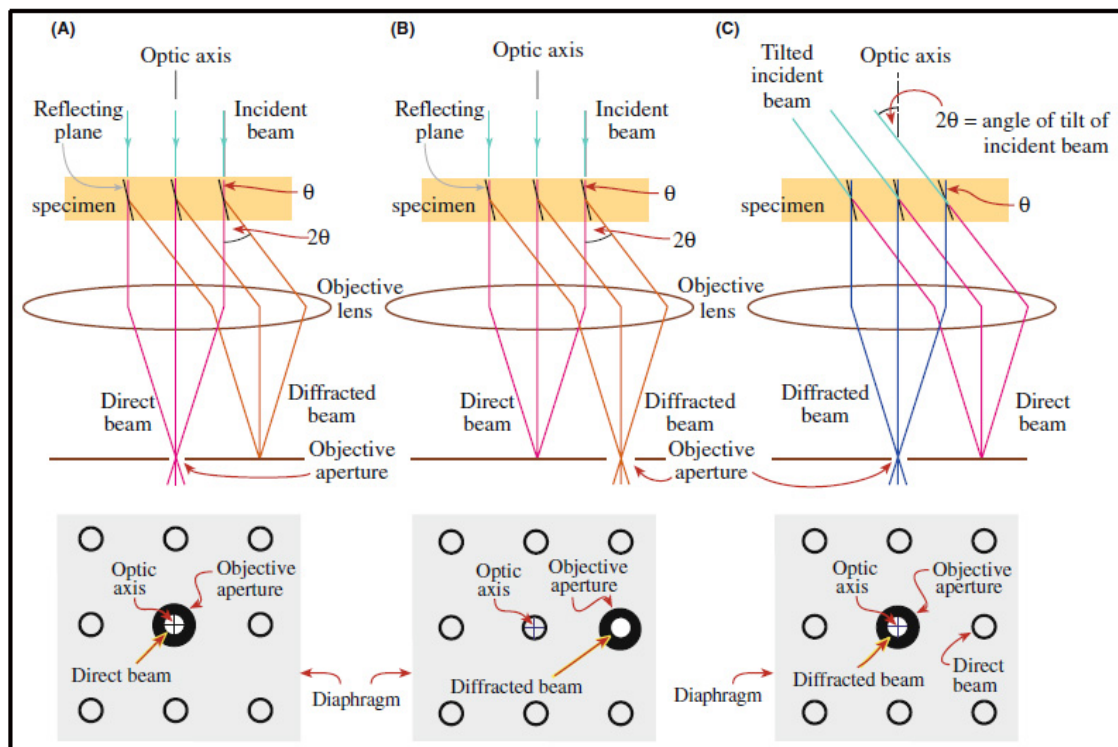


Figure 2.2: Schematic ray diagram illustration of TEM imaging modes. (A) Bright field imaging mode where only the forward electron beam is allowed through the objective aperture. (B) Dark field imaging mode operates while one diffracted beam is selected by the objective aperture. (C) Centered dark field imaging mode where objective aperture is placed on-axis and diffracted electron beam gets selected to give image contrast by tilting the incident electron beam [2].

Our *in situ* heating experiment is performed using centered dark field imaging in order to find the optimum diffraction orientation. This diffraction orientation can be interpreted in terms of the Bragg angle. The diffracted beams of this angle are collected by the objective lens giving one diffraction spot which is selected by the objective aperture placed at the center of the back focal plane, as shown in Figure 2.2 (C).

The Bragg angle can be calculated by the Bragg's law. In a crystalline sample,

the parallel incident electron beam is deflected by the atomic planes according to Bragg scattering. The Bragg's law is expressed as equation 2.1:

$$2 d_{hkl} \sin \theta = \lambda \quad (2.1)$$

where d_{hkl} represents the planar distance of atomic plane set (hkl) ; θ is the scattering angle and λ is the wavelength of the incoming electron wave.

3

Sample Preparation

In this chapter, preparations of the samples in this thesis work are discussed. Nanoscale indium islands for the *in situ* heating experiment are deposited on the silicon nitride film by thermal evaporation. For calibration of the TEM electron beam current, sharp gold tip is first made by electrochemical etching which is then fabricated into a custom Faraday cup using the FIB microscope.

3.1 Indium Islands

Nanoscale indium islands for the *in situ* heating experiment are deposited on top of the thin silicon nitride membrane. Silicon nitride is a hard material with high melting temperature (1900 °C for the most commercialized compound Si_3N_4 [10]). The electron beam transparent membrane is made to be 50 nm thick sitting on a 200 μm thick circular silicon substrate with a window of 250 $\mu\text{m} \times 250 \mu\text{m}$. The sample is obtained commercially from *Norcada* [11], which is shown in Figure 3.1.

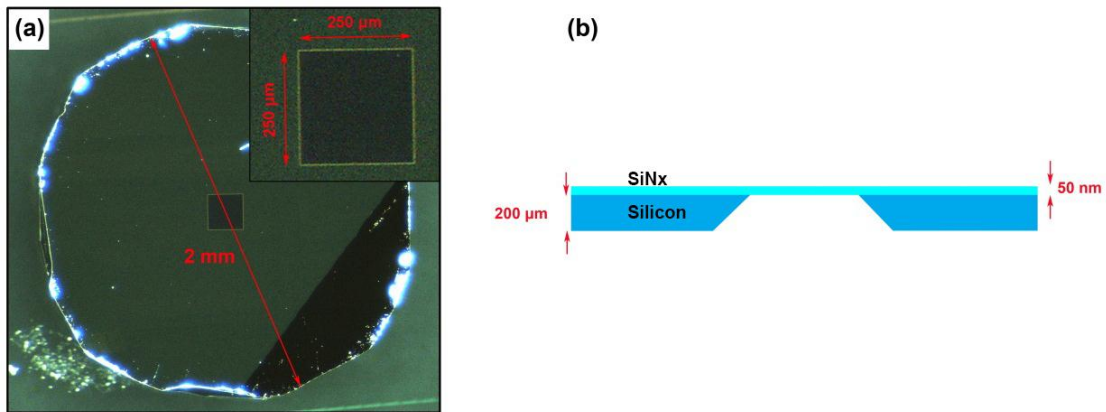


Figure 3.1: Electron beam transparent thick silicon nitride membrane with thickness of 50 nm lying on top of a 200 μm thick frame of silicon with a 250 $\mu\text{m} \times 250 \mu\text{m}$ transparent window for electron beam's passing through. The sample was brought from obtained from *Norcada* [11]. (a) is the top view optical micrograph. (b) is the schematic diagram of the cross section where the light blue represents the silicon nitride film and the dark blue is the silicon frame.

Indium is selected for the *in situ* thermal experiment due to its low melting point

3. Sample Preparation

which for the bulk of pure indium is 156.6 °C [12]. Indium islands are deposited on the silicon nitride film through metal evaporation in cleanroom by doctor Norvik Voskanian. The nanoscale indium island consists of a pure indium core with a thin indium oxide shell, as schematically illustrated in Figure 3.2.

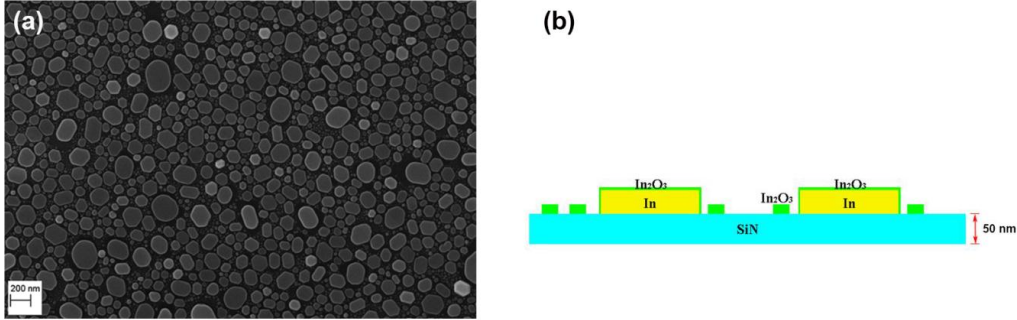
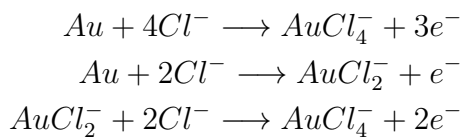


Figure 3.2: Nanoscale indium islands deposited on the silicon nitride thin film. (a) SEM image of indium islands deposited on the silicon nitride membrane. (b) Schematic diagram illustrating the indium islands deposited on the 50 nm thick silicon nitride membrane. Silicon nitride membrane is drawn in light blue. The indium islands are drawn with the indium core in yellow and the oxidized shell in green.

3.2 Sharp Gold Tip

To calibrate the current of the electron beam, a Faraday cup is needed. The Faraday cup is fabricated on a sharp gold tip that can be easily mounted into a TEM holder with electrical feedthroughs. In this section, details regarding the preparation of the sharp gold tip are discussed. As a typical method for gold tip fabrication, electrochemical etching has been heavily studied since the discovery of near-field optics [13–24]. However, reproducibility of tip quality has always been a problem.

In this experiment, parameters of electrochemical etching setup, such as immersion depth, gold wire diameter and etchant content, are taken into consideration to produce a reliable method for high quality gold tips. Gold tips with curvature radii of 20 nm are fabricated with high yield ratio and good reproducibility. According to references [13, 17], gold dissolves in concentrated hydrochloric acid (37% HCl) with following reactions taking place:



Strength of the direct current (DC), volatilization and consuming of HCl molecules are factors influencing the chemical reactions.

The experiment setup is schematically illustrated in Figure 3.3 (a). The anode is a gold wire immersed into the concentrated hydrochloric acid (37%). The cathode is a ring made of gold or platinum providing a cylindrical isotropic electric field to the anode. In this project, one-step and two-step etching approaches are used. The one-step etching is shown as Figure 3.3 (b). The anode gold wire is etched until the breaking of the taper with a formation of narrowed tip area. In the two-step etching, as illustrated in Figure 3.3 (c), the gold wire is first etched to give a taper which is not broken. In the second step, the immersion depth is increased which means the first etched region is further polished within the acid. Finally, the first taper breaks giving a sharp tip area with good smoothness.

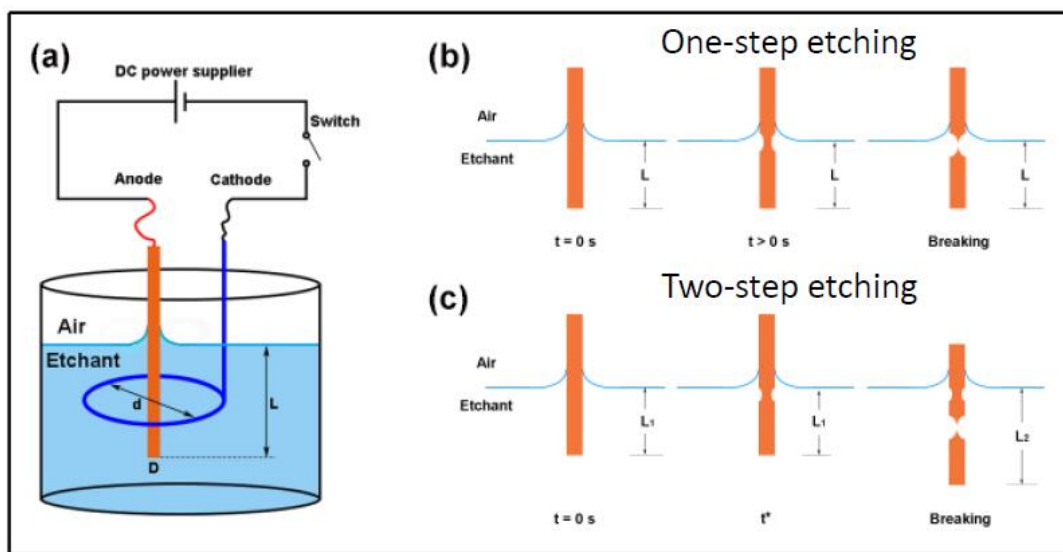


Figure 3.3: Schematic diagrams of the experiment setup and principles of the electrochemical etching process. (a) Schematic configuration of experiment setup for gold tip preparation based on electrochemical etching. The anode gold wire is immersed into the etchant solution based on concentrated hydrochloric acid (37%) together with the surrounding cathode providing a uniform electric field that is cylindrical isotropic under external bias provided by the DC power supply. (b) is the basic process of one-step etching method where gold wire is immersed into the etchant with a constant depth L and a tip apex is formed with dropping of lower part caused by narrowing of gold wire at the taper. (c) shows two-step etching process where gold wire is immersed into the etchant with L_1 at first to be etched for a time period as t^* , which is followed by an increment of immersion depth to be L_2 and finally tip is formed by the breaking at the first taper region.

3.3 Faraday Cup

Electron beam current is the crucial factor influencing the amount of beam heating so that the accurate measurement of the current value is necessary. In reference [4], beam current densities are estimated as the read-out given by the electron fluorescent screen which is not accurate. First, secondary electrons and back scattered electrons generated from the fluorescent screen are not included, which underestimates the beam current value compared to that of the primary beam. Second, lack of calibration also lowers the accuracy of the read-out value given by the TEM fluorescent screen. A TEM holder equipped with Faraday cup is commonly used to measure the electron beam current, which is schematically shown as Figure 3.4.

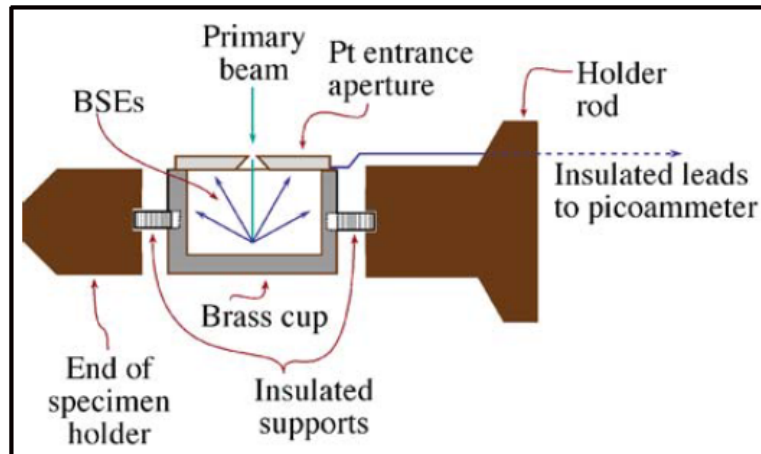


Figure 3.4: A schematics of a TEM Faraday cup [2] where a metallic chamber is covered by a small aperture for electron beam to pass through. Secondary electrons and back scattered electrons generated in the metallic chamber are blocked by the aperture diaphragm made of platinum. An insulated wire connects the chamber to a picoammeter which measures the value of incident beam current with high accuracy.

In reference [25], a SEM Faraday cup is made by FIB on a bulk metal. However, we decided to fabricate the TEM Faraday cup on the gold tip discussed in section 3.2, considering the geometric constraints of the pole piece and the goniometer. Dimensions of the Faraday cup fabrication in FIB-SEM is schematically shown as Figure 3.5. The bulk of the gold tip is first drilled by ion milling in FIB creating a blind hole of $30\ \mu\text{m}$ in diameter and $60\ \mu\text{m}$ in depth. Platinum is then deposited as ring patterns on top of each other step by step with diminishing diameters which gives an open hole of $5\ \mu\text{m}$ for receiving the incident electron beam. Three marks are made at the edge of the tip to help find the Faraday cup in TEM as indicated as the arrows in Figure 3.5 (a) and (e).

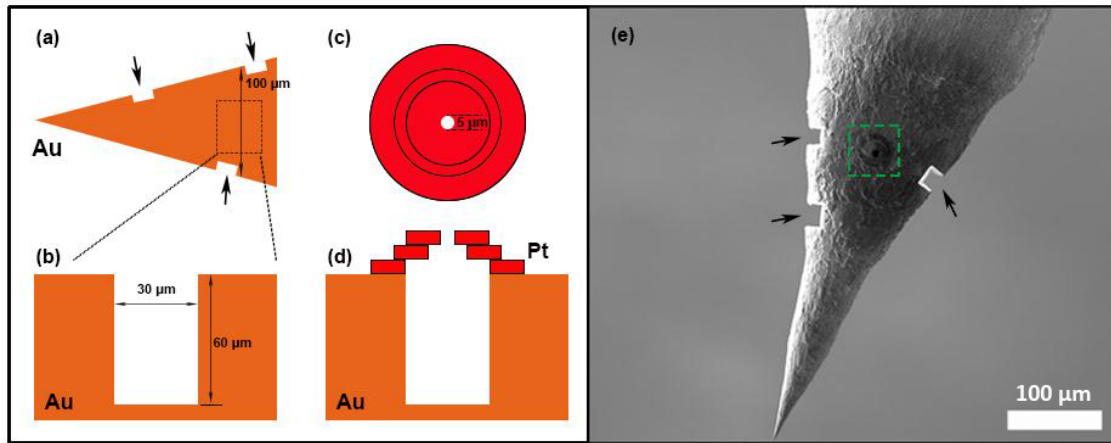


Figure 3.5: Dimensions of the Faraday cup fabrication by FIB - SEM. (a) represents the area on the gold tip with diameter of $100 \mu\text{m}$ that is chosen for the ion milling. A blind hole with diameter of $30 \mu\text{m}$ and $60 \mu\text{m}$ deep is drilled by ion beam, as illustrated in (b). (c) is the illustration of platinum deposition patterns where platinum is deposited as rings on top of each other step by step that gives an open hole for primary electrons with $5 \mu\text{m}$ in diameter. (e) SEM image of the Faraday cup on the gold tip. Arrows are the marks that help to find the cup regions marked by green box.

3. Sample Preparation

4

Thermal Experiment

In this thesis work, the *in situ* heating experiment on nanoscale indium islands is performed by the centered dark field TEM imaging. The electron beam current is measured by the custom Faraday cup and a picoammeter setup. The electron beam current density is calibrated by measuring the illumination area using a standard TEM grating sample.

4.1 Electron Thermal Microscopy

The *in situ* heating experiment on multiple nanoscale indium islands through dark field imaging is called EThM, proposed by Brintlinger *et al* [7]. Basic principles of EThM are illustrated in Figure 4.1. In the dark field imaging, the objective aperture is placed at the position as shown in Figure 4.1 (b), (c) and (d) indicated by a white circle, which corresponds to the Bragg angle that is available for the liquid phase of indium but not for the solid ones. When the solid to liquid phase transition happens, the image contrast of indium island changes from dark to bright due to the electron scattering from the liquid phase.

In our project, centered dark field imaging mode is used. In contrast to dark field imaging, the objective aperture is located at the center of the back focal plane of the objective lens. The primary beam is tilted so that the electron diffracted with the same Bragg angle is collected by the aperture.

4.2 Heating Holder

The *in situ* heating experiment is performed using a special TEM heating holder, as shown in Figure 4.2. As seen in Figure 4.2 (a), a tungsten heating wire (B) is placed on the back side of an oven (C) made of platinum. The front side of the holder is shown as Figure 4.2 (b). The sample to be studied is placed inside of a groove in the heating oven, which is mechanically stabilized by a metallic washer and a spring. Thermocouple (D) is connected to the heating oven measuring the temperature and sending signals to a feedback loop to stabilize the temperature to the value that is preset externally.

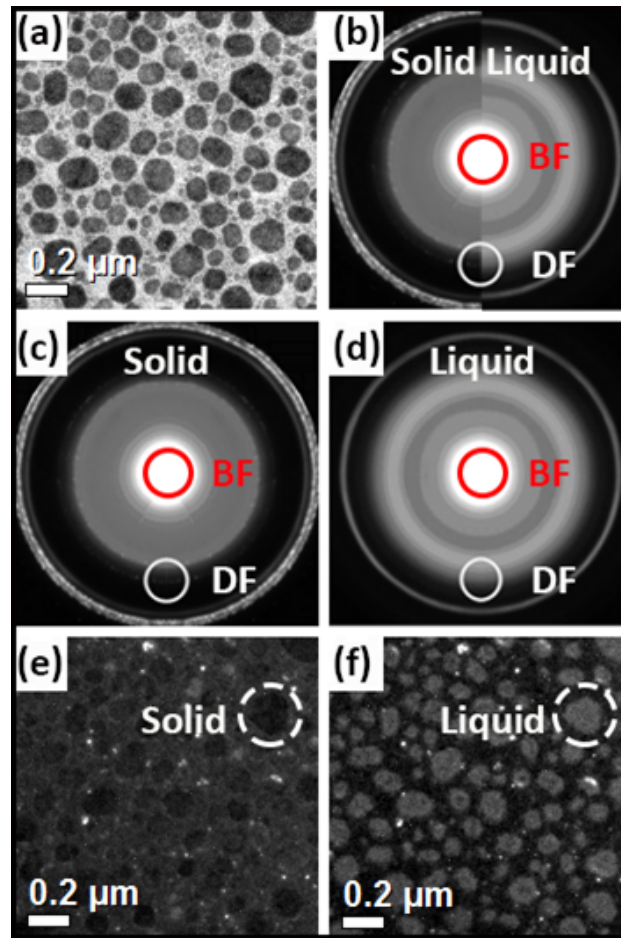


Figure 4.1: Dark field imaging on indium solid to liquid phase transitions [7]. (a) shows the bright field image of indium islands under room temperature. (b) is a composite diffraction pattern of the indium islands in solid and liquid phases [7]. The white circle is the position of select area aperture where diffracted beam is collected for the dark field imaging. (c) is the diffraction pattern of solid indium islands [7]. (d) is the diffraction pattern of molten indium islands [7]. (e) and (f) are the dark field images of solid and liquid islands respectively where a sudden contrast change in the island pixels corresponds to the liquid-solid phase transition. Scale bar is 200 nm.

4.3 Heating Process

Considering the hysteresis effect of melting temperature, heating process of the experiment is kept invariant. First, the correct beam condition for the centered dark field imaging is found by heating the sample from room temperature to 180 °C by at a rate of 10 °C per every 10 minutes where the electron beam is tilted slightly to find the correct Bragg angle for observing the contrast shift when the solid to liquid phase transition happens. After finding the correct Bragg angle, the sample is then cooled down to room temperature by at a rate of 10 °C per 10 minutes. Second, the *in situ* heating experiment is performed followed the heating process as shown in Figure 4.3.

As shown in Figure 4.3, the sample is first stabilized at 60 °C for 15 minutes . The sample is heated to 100 °C with heating speed as 10 °C per 5 minutes . At each heating step, another 2 minutes are saved for imaging acquisition. Above 100 °C, the heating speed is slowed down to 5 °C per 5 minutes to get more data spots. The melting of indium islands usually happens between 100 °C and 130 °C.

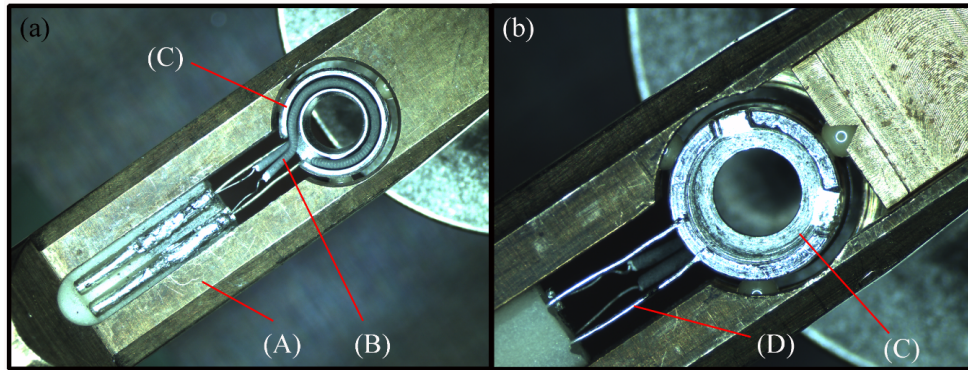


Figure 4.2: TEM holder for the *in situ* heating experiment. (a) is the front side of the heating holder where the frame rod, heating wire made of tungsten and the heating oven made of platinum are marked as (A), (B) and (C) respectively. (b) is the back side of the holder where (D) is a pair of thermal couple for temperature measurement.

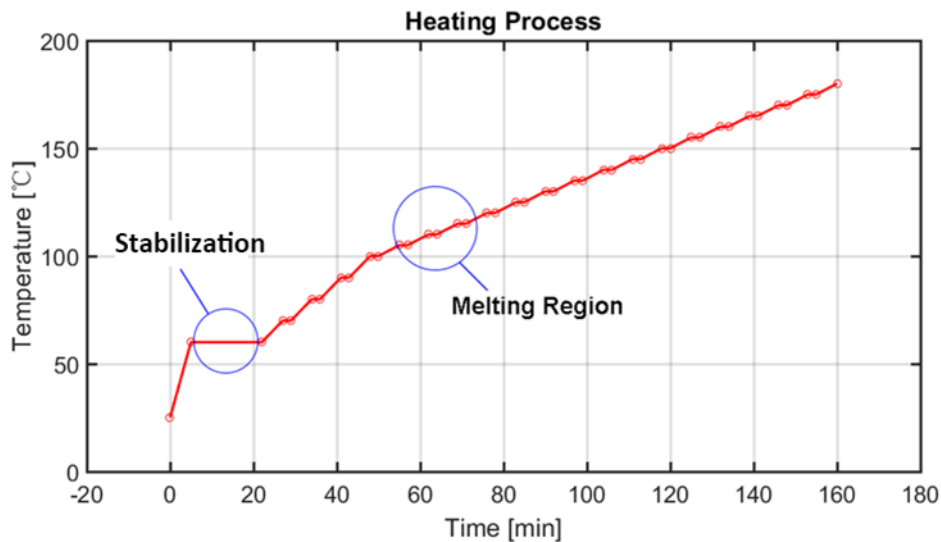


Figure 4.3: Heating process of the *in situ* experiment after the determination of beam tilting angle of the centered dark field imaging. The specimen is heated up from room temperature to 60 °C and stabilized for 15 minutes. The melting region of indium islands is found to be between 100 °C and 130 °C following this heating process depending on the island size and the electron beam condition.

4.4 Electron Beam Calibration

The area on the sample illuminated by the electron beam is calibrated by a standard cross grating sample from *Agar Scientific* [26] as shown in Figure 4.4 (a). One example of the projection of illuminated sample area on the fluorescent screen is shown in Figure 4.4 (b). The size of illumination is determined by counting the number of grids.

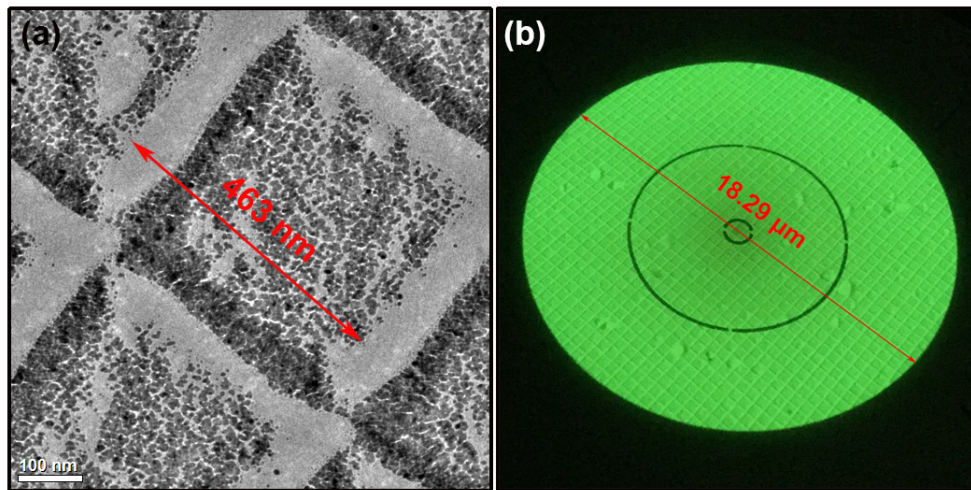


Figure 4.4: Illumination area calibration using the standard cross grating sample from *Agar Scientific* [26]. (a) shows that the size of one grid is 463 nm. (b) is an image of the illuminated area projected on the fluorescent screen indicating a diameter of 18.29 μm by counting the number of periodic grids. The image is taken by phone camera.

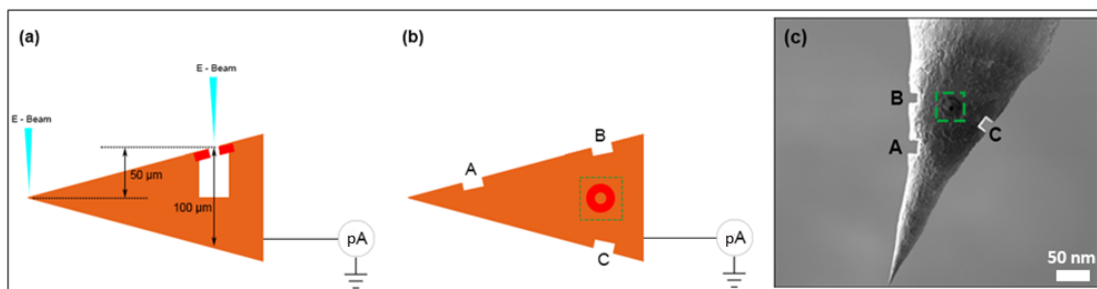


Figure 4.5: Illustration of the beam current measurement. (a) is the side view where the electron beam is first focused at the tip front. The eucentric height is lowered by 50 μm to align the height of the beam spot with respect to that of the Faraday cup aperture. (b) is the top view. Three marks A, B and C are made by ion milling at the edge of the tip to help adjust the orientation of the tip and find the cup aperture. (c) shows the SEM image from the top view.

As mentioned in chapter 3, a custom Faraday cup is fabricated to measure the beam

current in TEM. The measurement of the beam current is illustrated as Figure 4.5. The tip with the Faraday cup on is mounted on a *Nanofactory* holder with an electrical feedthrough connecting to a picoammeter. As shown in the side view of the tip, see Figure 4.5 (a), the electron beam is first focused at the front of the tip to find the eucentric height. Next the tip is lowered by $50\ \mu\text{m}$ to align the height of the beam spot to that of the Faraday cup aperture. The tip is then moved laterally where the position of the cup aperture can be found with the help of the marks (A, B and C) as shown in the top view of the gold tip, see Figure 4.5 (b).

5

Image Analysis

For more efficient and accurate data analysis, MATLAB imaging processing is implemented on the TEM bright and dark field images. The image processing applied in this project includes OTSU thresholding, watershed segmentation and image alignment. The MATLAB codes can be found in the appendix section.

5.1 OTSU Threshold

To automatically distinguish the indium islands from the background substrate, image threshold is applied to the bright field image, Figure 5.1. The algorithm used known as OTSU thresholding, first proposed in 1979, named after the Japanese computer scientist Nobuyuki Otsu [27]. Assuming L gray scale levels $[1, 2, \dots, L]$ in a grey scale image. Define the number of pixels with intensity level i as n_i where the total pixel number in this image is $N = n_1 + n_2 + \dots + n_L$. The probability distribution is normalized as:

$$p(i) = n(i)/N \quad (5.1)$$

where p_i represents the probability of finding one pixel belonging to the gray scale level labeled as i .

From the image histogram, the pixel intensity spread of the indium islands and the silicon nitride can be separated optimally by means of choosing the threshold value T through minimizing an ensemble variance defined as:

$$\sigma_{en}^2(T) = \sigma_{In}^2(T) \cdot \sum_{i=1}^{T-1} p(i) + \sigma_{SiN_x}^2(T) \cdot \sum_{j=T}^L p(j) \quad (5.2)$$

where $\sigma_{In}^2(T)$ and $\sigma_{SiN_x}^2(T)$ represent the gray level variance of pixels belonging to the class defined as indium islands and silicon nitride background respectively, which can be calculated from the definition as:

$$\sigma_{In}^2(T) = Var\{i, 1 \leq i < T\} \quad (5.3)$$

$$\sigma_{SiN_x}^2(T) = Var\{j, T \leq j \leq L\} \quad (5.4)$$

The OTSU threshold algorithm is encoded in MATLAB in its image processing toolbox, as shown in the appendix. The function of OTSU threshold is shown in Figure 5.1, where a threshold value is determined to be 0.5608, above which the pixels

are classified to be silicon nitride and below which the pixels are considered belonging to indium islands, indicated by the white area in Figure 5.1 (b).

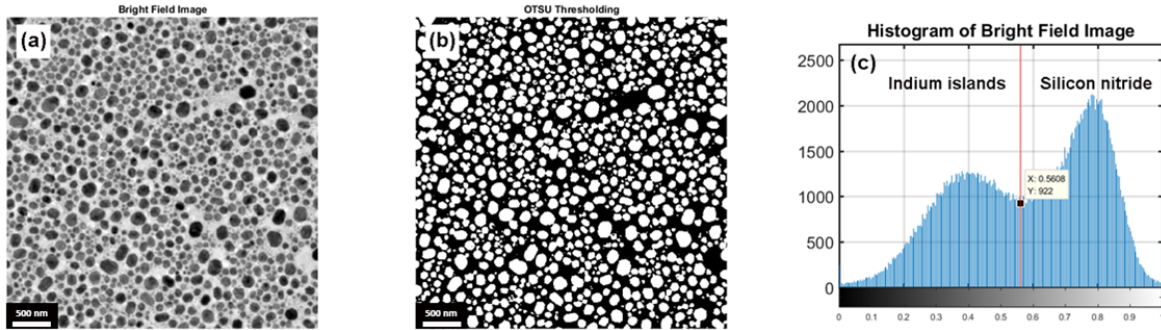


Figure 5.1: OTSU thresholding result of the bright field image. (a) TEM bright field image in gray scale. (b) Binary image obtained from OTSU threshold. (c) Pixel intensity histogram of the bright field image where the optimal threshold is calculated as 0.5608 from OTSU algorithm. Pixels with intensity above this threshold is classified as silicon nitride and the ones with intensity lower than this threshold are categorized into that belonging to the indium islands.

5.2 Watershed Segmentation

After the OTSU threshold process, the bright field image is transferred into a binary image as shown in Fig. 5.1 (b). The bright pixels belong to indium islands and dark pixels are classified as background. A further segmentation process is used to separately count islands that appear to be connected, as seen in Fig. 5.1 (b). In this project, the Watershed segmentation is applied, which was first proposed in 1979 by Beucher, *et al* [28, 29].

Starting with the binary image as shown in Figure 5.2 (a), the distance transform is first performed, which gives the distance transform image as seen in Figure 5.2 (b). In the distance transform image, the intensity of each island pixel is proportional to the distance between this pixel and the nearest background pixel [30]. A three dimensional plot of Figure 5.2 (b) is shown in Figure 5.2 (c) where the lower the pixel intensity in image Figure 5.2 (b) the lower level in vertical dimension it is in Figure 5.2 (c). Thus, the two connected indium islands can be thought as two water catchment basins sharing a watershed. To simply illustrate the segmentation process, one can imagine that water droplets falling upon each pixel will fall by gravity into a certain local minima or a catchment basin. According to this, two islands are segmented pixel by pixel.

The result of watershed segmentation is shown in image Figure 5.2 (d) where pixels in yellow represent the edge of islands and the ones in brown are the ones belonging to corresponding indium islands. Pixels in blue represent the background. Functions of distance transform and watershed segmentation are encoded in MATLAB.

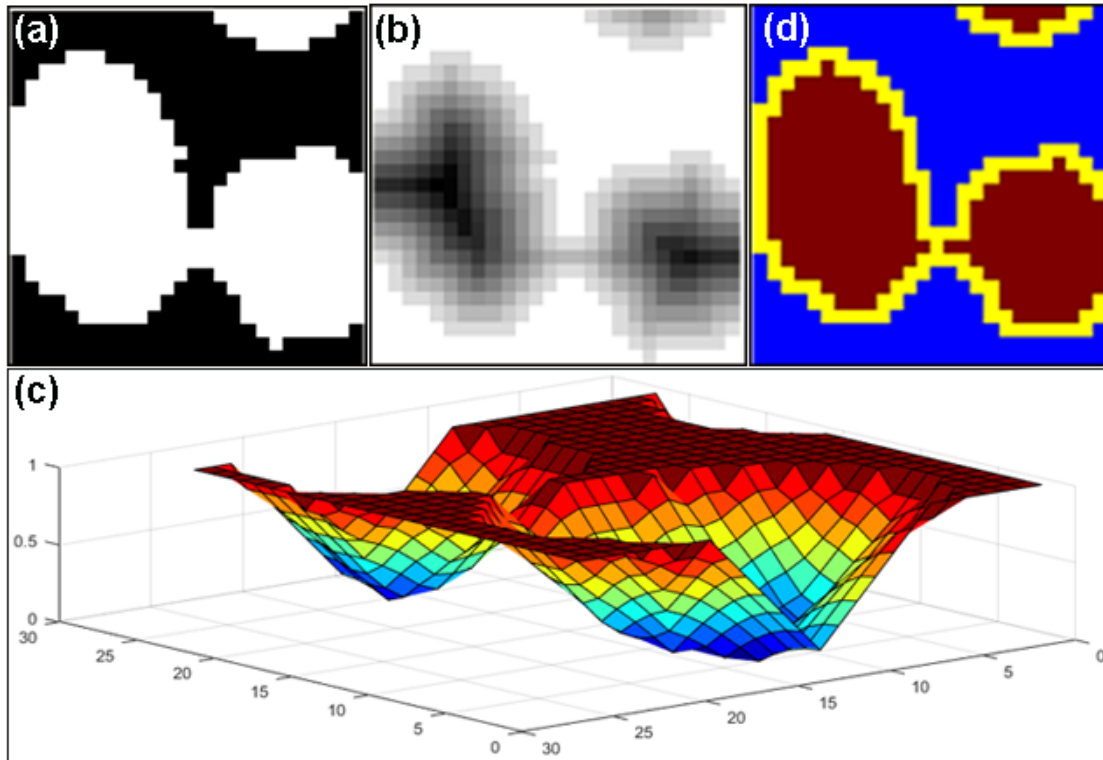


Figure 5.2: Example of the watershed segmentation. (a) Initial binary image obtained from bright field image through OTSU threshold. (b) Distance transform of (a). (c) Three dimensional plot of distance transform where two catchment basins where represent the corresponding islands. (d) Result of watershed segmentation where pixels in yellow represent the edge and the ones in brown are that of indium islands. Pixels in blue represent the background.

5.3 Image Alignment

After the OTSU thresholding and watershed segmentation, indium islands are identified in the bright field image. To locate the indium islands in dark field images, misalignment of all images caused by the sample drifting during the *in situ* heating experiment is corrected. Alignment between dark field image and the bright field image is done through continuously shifting the images until no obvious misalignment exists. Alignment between the dark field images is done as illustrated in Figure 5.3. A bright feature corresponding to small indium oxide particle is indexed manually in each image, labeled as A or B in Figure 5.3. All dark field images are rigidly aligned by overlapping the bright spots in each image.

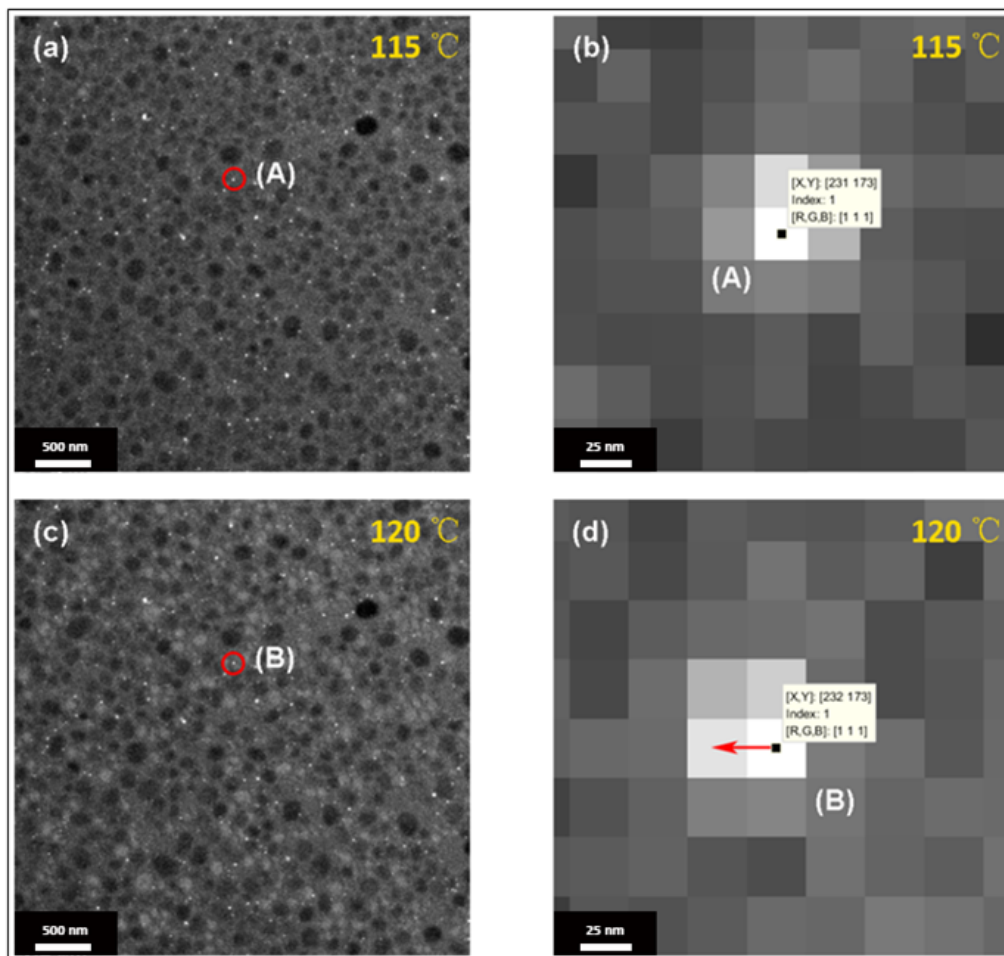


Figure 5.3: Illustration of the dark field image alignment. (a) and (c) is the dark field image under 115 °C and 120 °C. A tiny bright feature of the indium oxide nano particle is marked out by the red circle whose positions in (a) and (c) are shown in sub-figure (b) and (d) respectively. The red arrow in (d) means that the dark field image (c) should be rigidly shifted towards left by one pixel to align well with respect to image (a).

6

Results

In this chapter, the results of this master thesis project are discussed. First, the gold tips made from electrochemical etching and the Faraday cup fabricated by FIB-SEM are shown, which gives the calibration of the TEM beam current. Second, result of the image processing on indium islands identification is discussed. Finally, the results of the *in situ* heating experiments and the beam heating effect are discussed.

6.1 Gold Tip

As described in chapter 3, sharp gold tips are prepared by electrochemical etching method where the one-step and two-step approaches are studied. The one-step etching is more efficient but the two-step etching gives gold tips with better smoothness.

6.1.1 One - step Etching

In one-step etching approach, gold wire with diameter of 250 μm is used, which is immersed vertically into the mixture of concentrated hydrochloric acid (37 %) and ethanol (99.7 %) with an immersion depth of 2 mm, as schematically illustrated in Figure 3.3.

Constant DC bias of 2.4 volts (V) is applied by an *EL561R* power supply during one-step etching process. However, it is found that gold tips are of low reproducibility and bad quality. In most cases, these tips are blunt and the apical radii are of micrometer scale. Some tips show multi-tip structures, as seen in Figure 6.1 (a). This is thought to be due instability of the electrical potential provided by the power supply. Therefore, a commercial potentiostat, *Gamry Interface 1000*, operated in the *Physical Electrochemistry* mode is used to produces smooth and sharp gold tips. As shown in Figure 6.1 (c), a smooth gold tip with 34 nm apical radius is made with DC bias of 2.4 V applied by the potentiostat. Gold tip with smaller curvature radius is made when the immersion depth is reduced to 1 mm, as seen in Figure 6.1 (b).

The kinematic reaction rate is explained by the diffusion-coupled periodic current oscillation model [13,24] from the creation and depletion of product ions around the interface between the gold wire and the solvent. As shown in Figure 6.1 (d) and (e), etching current drops to nano-ampere (nA) regime after the breaking of taper, which is of the same scale of the background current as plotted in Figure 6.1 (f).

6.1.2 Two - step Etching

In the two step etching process, recipe of gold wire with diameter of 250 μm and 1:1 mixture of concentrated hydrochloric acid (37 %) and ethanol (99.7 %) is tried. DC voltage of 2.4 V is applied by potentiostat *Gamry Interface 1000*.

In the two-step etching, the gold wire is first etched with immersion depth of 1 mm. It causes the reduction of cross section area in this taper. In the second step, immersion depth is increased to 2 mm. The gold wire is then etched until the breaking of the first taper. In the example shown in Figure 6.2, the first and second etching steps take 390 s and 95 s respectively. As shown in Figure 6.2, sharpness of the tip is sacrificed in the two-step etching for increased smoothness due to the polishing effect in the second step.

In this project, the gold tip used for the fabrication of the Faraday cup is not influenced its sharpness. However, high quality tips are in great demand in many research fields. Sharp and smooth tips play important roles as microprobes in scanning tunneling microscope (STM) [13,31,32], atomic force microscope (AFM) [33], *in situ* TEM [34], atom probe tomography experiment [35] and nanofabrication technique, like dip-pen nanolithography [36,37]. Gold and silver tips are more important due to their chemical inertness and high density of near-free electrons. It gives rise to an enhancement of the near field component of electric field and the local surface plasmon (LSP) excitations, which is the key element of tip enhanced Raman spectroscopy (TERS) [13] and near field optical techniques such as aperture-less near field scanning microscope (NSOM) [38].

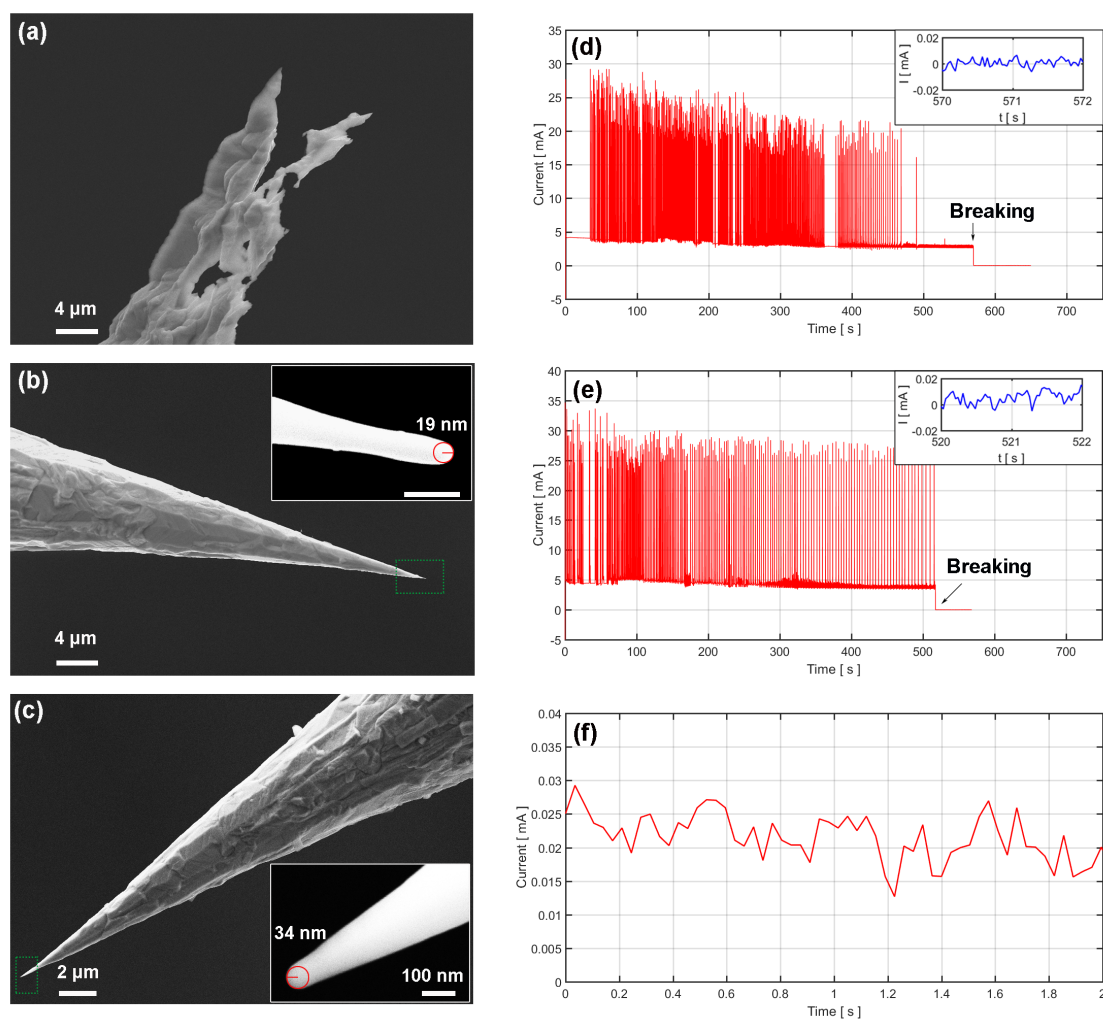


Figure 6.1: Images and corresponding etching current variations of tips made from one-step etching method by gold wire with $250\ \mu\text{m}$ diameter. The etching solution is a mixture of concentrated hydrochloric acid (37%) and ethanol(99.7%) with 1:1 volume ratio. DC voltage of 2.4 V is applied between the anode and cathode sides. (a) shows a typical gold tip made by a *EL561R* power supply with immersion depth of 1 mm. (b) shows the image of a gold tip produced by immersion depth of 1 mm under DC bias 2.4 V provided by a commercial potentiostat *Gamry Interface 1000* under *Physical Electrochemistry* mode. (c) shows a image of tip made with same parameters as (b) but only increasing the immersion depth from 1 mm into 2 mm. Plot (d) and (e) give periodic variations of etching current corresponding to the tips shown as (b) and (c) respectively. Etching current after breaking of meniscus is shown in the reduce window. (f) gives the typical value of background current of the etching system with open circuit.

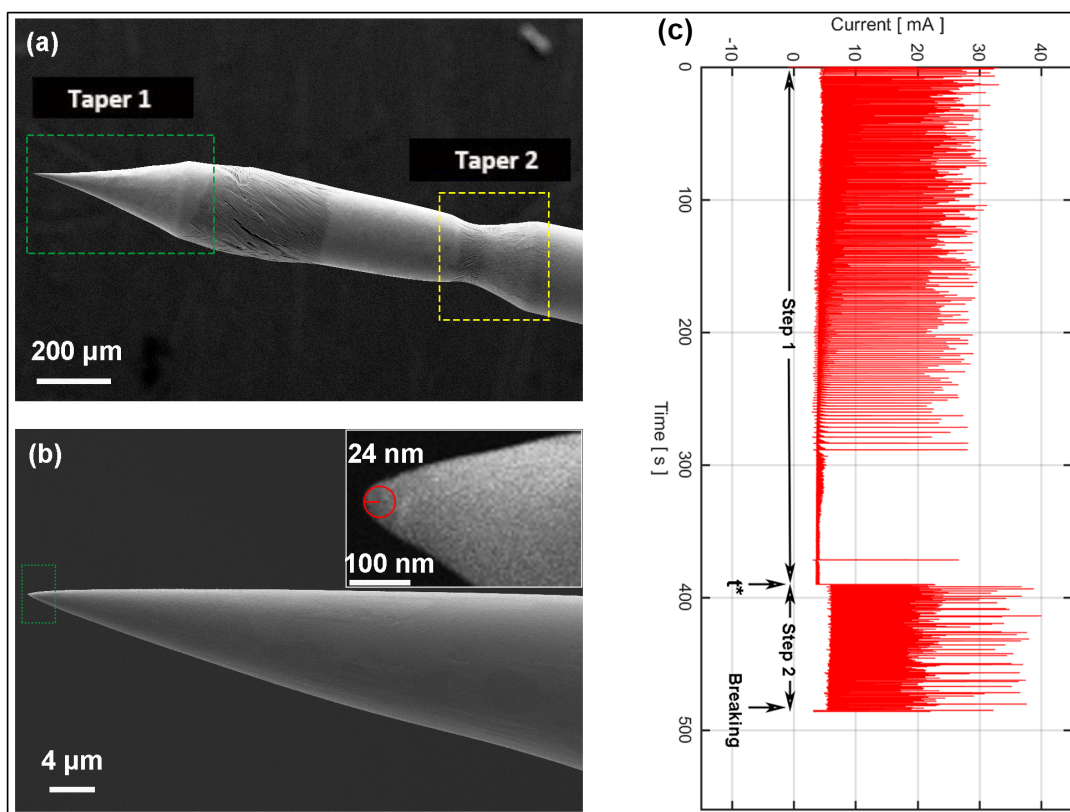


Figure 6.2: Gold tip prepared through two-step etching method. (a) Tip region is formed at taper 1 marked by the green rectangular box. The yellow box shows the taper 2 formed during the second step etching. (b) shows the corresponding tip at taper 1, which is extremely smooth over a large spatial scale but with the sharpness sacrificed. (c) Etching current variation of two step etching. Gold wire has diameter of $250\ \mu\text{m}$. Commercial potentiostat *Gamry Interface 1000* provides 2.4 V DC voltage by *Physical Electrochemistry* mode. In the first step, immersion depth is 1 mm and etching time (t^*) is chosen to be 390 s. In the second step, immersion depth is increased to be 2 mm and taper 1 breaks after another 95 s.

6.2 Homemade Faraday Cup

The Faraday cup fabricated by FIB method is shown as Figure 6.3. The tip is mounted in the TEM holder with optical microscope where the aperture of the Faraday cup is aligned facing up. Since the gold tip is too thick to be electron transparent alignment markers are used to locate the center of the Faraday cup. Three marks (A, B and C in Figure 6.3 (a)) are drilled by ion milling to help orient the aperture with respect to the electron beam and find the Faraday cup aperture. The position of the cup aperture is in the middle of marks A and C. Electron beam is moved slightly with respect to the sample until the maximum current signal is measured. Details of the cup aperture is shown in Figure 6.3 (b). Step-by-step deposition of platinum makes it possible to create a $5\ \mu\text{m}$ aperture covering a large vacuum bulk, details of the fabrication process have been discussed

earlier in chapter 3.

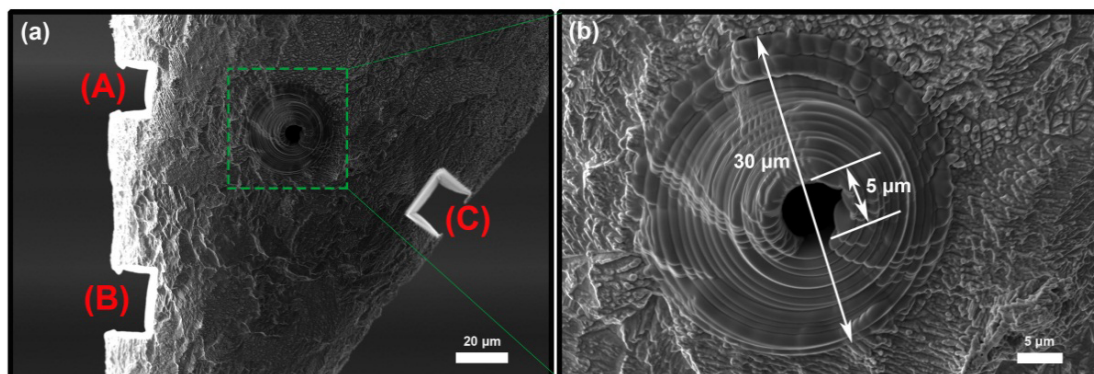


Figure 6.3: SEM images of the Faraday cup made by FIB - SEM method. In sub-diagram (a), three rectangles are milled to help determine the orientation of the gold tip in the TEM. (b) shows the structure of the Faraday cup where the aperture is made by platinum deposition.

6.3 Beam Current Calibration

Beam current is calibrated by the homemade Faraday cup placed in *Nanofactory* TEM holder where a picoammeter is connected with the gold wire. Fourier filtering is applied to reduce the noise in the measurements, as illustrated in Figure 6.4.

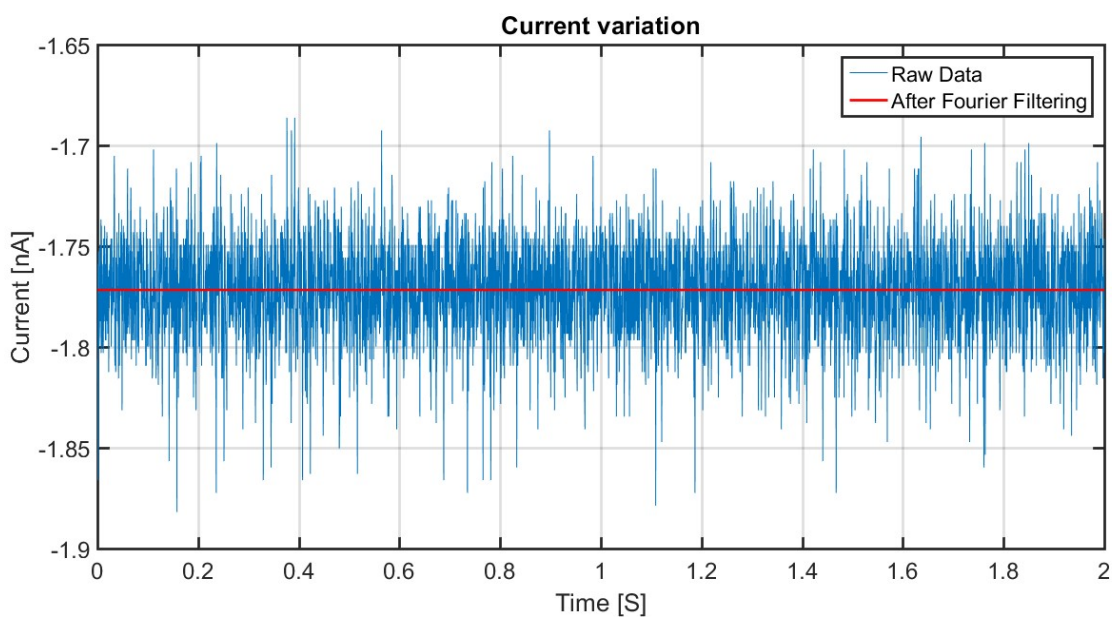


Figure 6.4: Example of the electron beam current calibration by the homemade Faraday cup and the picoammeter in a *Nanofactory* TEM holder. Random noise is eliminated by Fourier filtering.

A linear relationship, between the beam current measured by the Faraday cup and the one given by the TEM fluorescent screen read-out, is discovered. The coefficients are 1.2716, 1.1983 and 1.1499 for acceleration voltages as 200 kV, 120 kV and 80 kV, as shown in Figure 6.5.

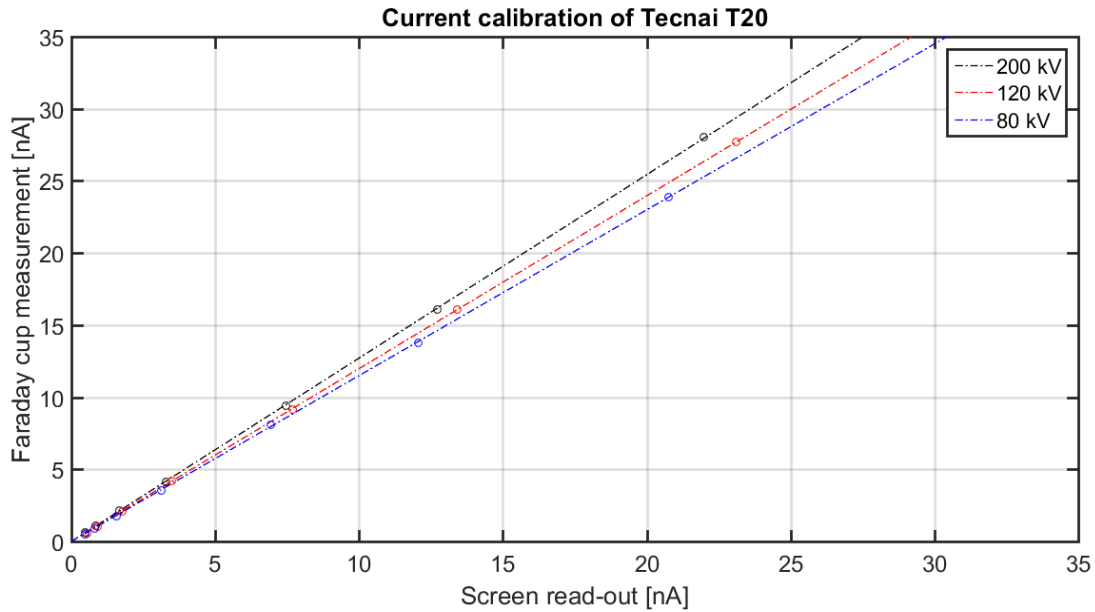


Figure 6.5: Calibration of beam current of the Tecnai T20 TEM. The linear coefficients between the current value given by the fluorescent screen of the TEM and the value measured by the homemade Faraday cup are 1.2716, 1.1983 and 1.1499 for the acceleration voltages to be 200 kV, 120 kV and 80 kV respectively.

6.4 Island Identification

Indium islands are identified and localized in the bright field image through OTSU threshold and watershed segmentation as discussed in chapter 5. Result of the identification of indium islands is shown in Figure 6.6 where (a) is the bright field image and (b) is the processed image after the OTSU thresholding and watershed segmentation.

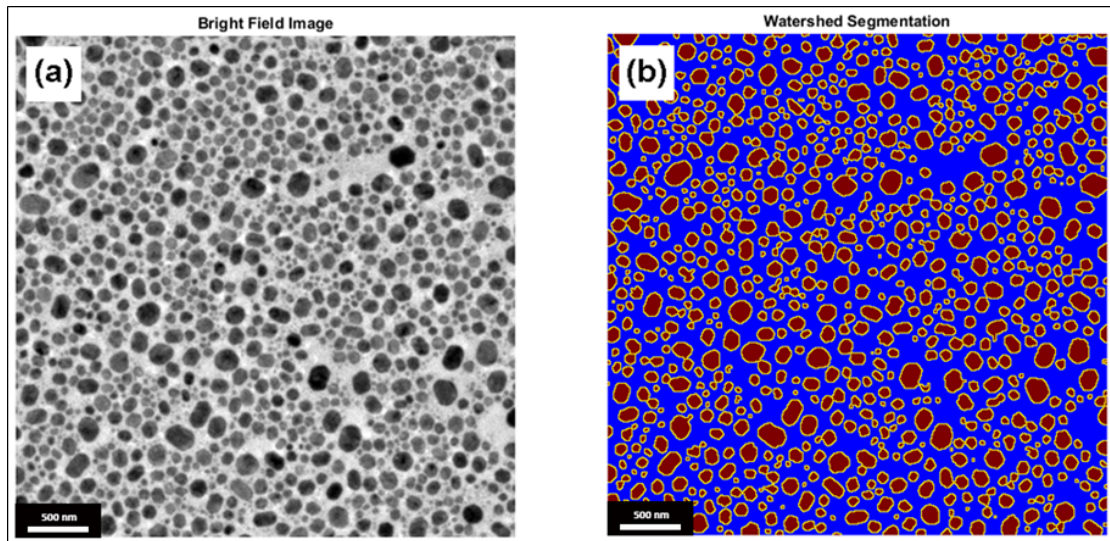


Figure 6.6: Indium island identification result from the OTSU thresholding and watershed segmentation. (a) TEM bright field image. (b) Island identification after applying the OTSU thresholding and watershed segmentation on the bright field image (a).

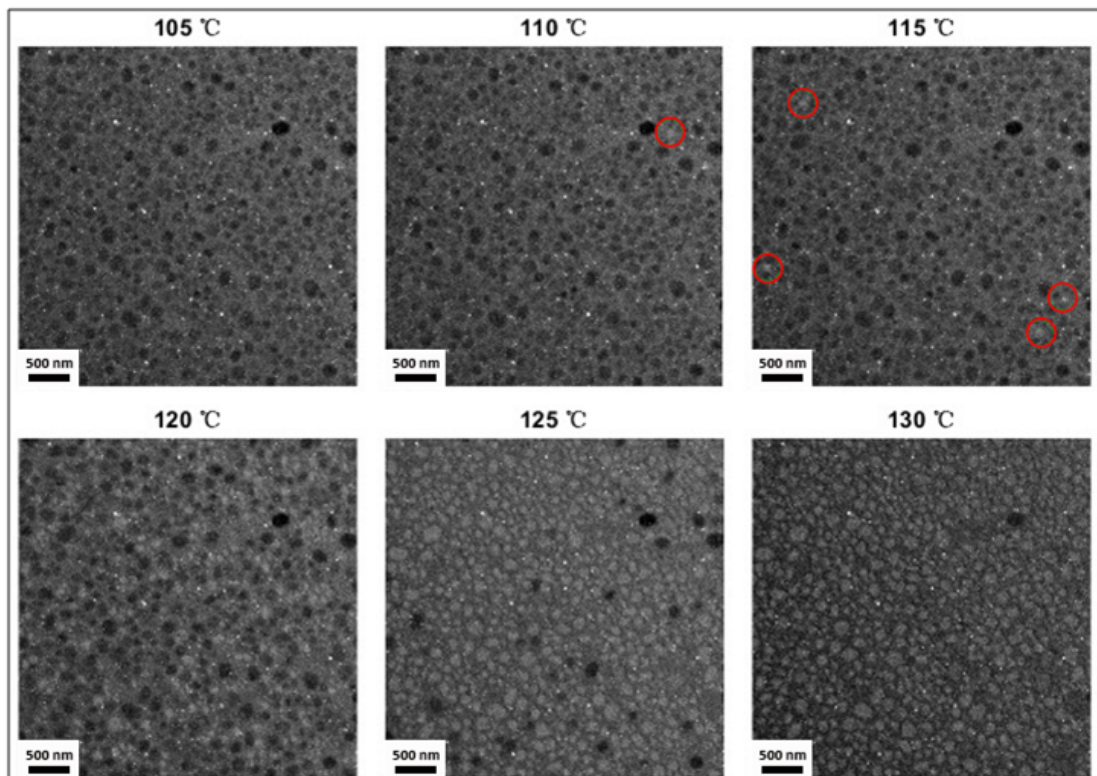


Figure 6.7: Melting process recorded through TEM dark field imaging. The melting process happens from 110 °C to 130 °C. The indium islands melted at 110 °C and 115 °C are marked by green circles.

The melting process is recorded through dark field imaging. An example of the

melting process is shown in Figure 6.7 where the number of molten islands increases as the temperature is increased from 110 °C to 130 °C. The solid to liquid phase transition of indium is indicated by the change of pixel intensity, from dark to light.

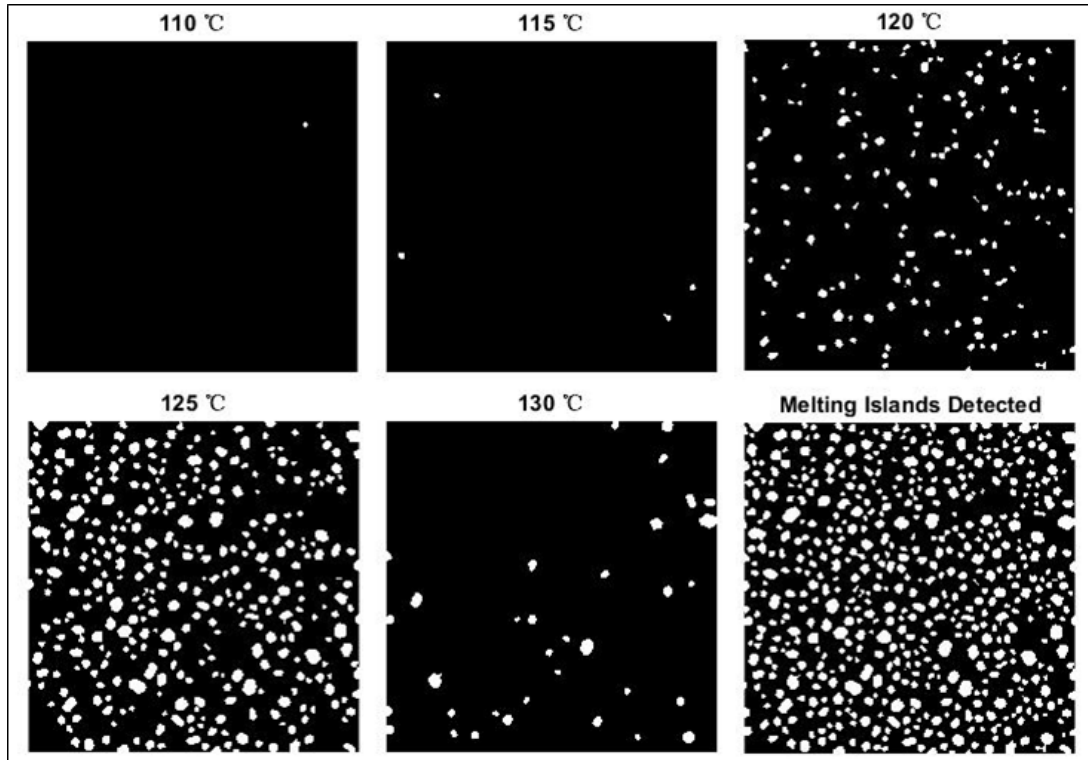


Figure 6.8: Melting process shown by binary images. The same melting process is shown by the dark field images in Figure 6.7.

Based on the identification and localization of indium islands, the melting of indium island can be recognized by change in pixel intensity during the heating process. By detecting the melted indium islands at each heating temperature, the melting sequence plot shown as the binary images as Figure 6.8 is given. In each frame of Figure 6.8, the indium islands molten in previous steps are removed which only gives the molten islands at each heating temperature. After the identification of indium islands, the size and location of each indium island are thus determined with pixel accuracy.

6.5 Electron Beam Heating

Since we have calibrated the electron beam current and identified the solid to liquid phase transition of indium islands, the relative electron beam heating effect can be estimated from the change of melting temperatures of indium islands with different beam conditions. Table 6.1 shows the TEM beam parameters of the *in situ* heating experiments, including the TEM acceleration voltage [HT], primary beam current

[I], illumination area [A], the calibrated electron beam current [\hat{I}] and the electron beam current density [i]. The beam current is varied by changing spot size and the illumination area is controlled by the focus setting of the condenser lens C2.

Table 6.1: Parameters of the *in situ* melting experiments.

<i>Experiment</i>	HT [kV]	I [nA]	\hat{I} [nA]	A [μm^2]	i [nA/ μm^2]
<i>E1</i>	200	17.20	21.87	26.70	104.2
<i>E2</i>	200	8.690	11.05	7.425	189.2
<i>E3</i>	200	4.500	5.722	7.145	80.09
<i>E4</i>	200	2.420	3.077	26.70	11.53
<i>E5</i>	200	0.290	0.369	26.70	1.417
<i>E6</i>	120	6.100	7.310	26.70	27.38
<i>E7</i>	120	3.530	4.230	26.70	15.84
<i>E8</i>	120	0.880	1.060	26.70	3.967

Assuming that the melting temperature of an indium island with a specific size is a constant (T_{melting}), the electron beam heating (ΔT) can then be obtained from the temperature provided by the heating holder (T_{holder}) at the melting point, according to equation 6.1:

$$\Delta T = T_{\text{melting}} - T_{\text{holder}} \quad (6.1)$$

The holder temperature at the melting point of indium islands with a diameter of 100 nm as a function of electron beam current is shown in Figure 6.9. Linear regressions are performed for experimental data for acceleration voltages of 120 kV and 200 kV.

An increase of electron beam heating is evidenced by the decrease in holder heating temperature. The regression shows that the electron beam heating is proportional to the primary electron beam current. A 15 °C beam heating is expected for 200 kV experiments at beam currents as high as 20 nA, see Figure 6.9.

The effect of the illumination area on the melting temperature is also taken into consideration. The method to measure the size of the illumination area is discussed in section 4.4. The effect of the illumination area has been discussed previously [1]. It was found that the illumination area has little influence on the beam heating in TEM. Similarly, our results indicate that it is the beam current instead of the illumination area that is the dominant factor giving rise to the specimen heating.

As shown in Figure 6.10, the data point marked as E2 gives more beam heating with less beam current density compared to E1 because of its higher beam current value.

6. Results

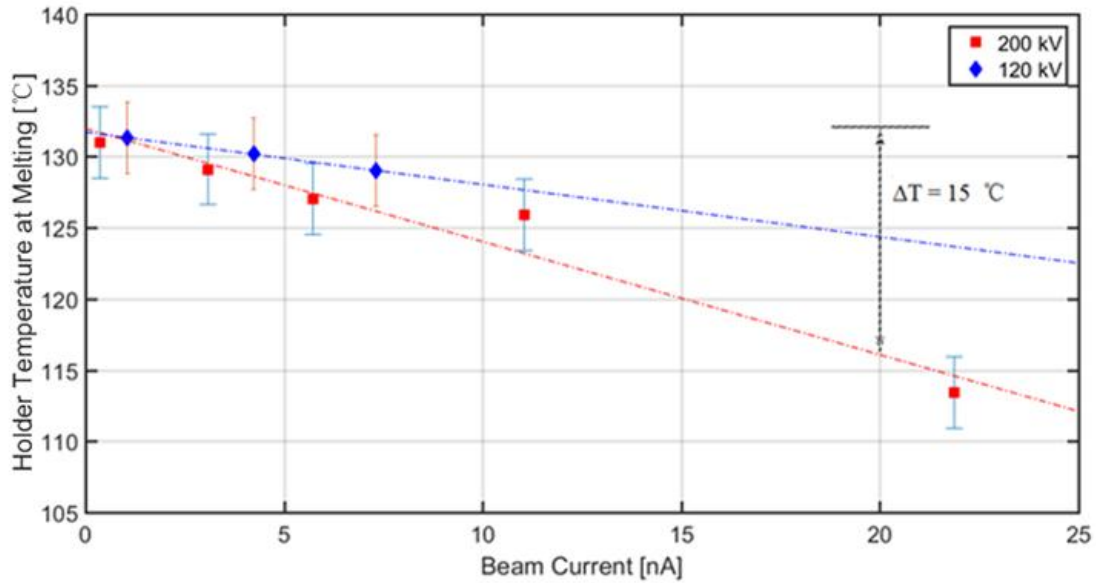


Figure 6.9: Holder temperature at melting point as a function of primary beam current at 120 kV and 200 kV acceleration voltages. The island diameter is 100 nm. The error bars are estimated to be 5 °C which is half of the interval between heating steps.

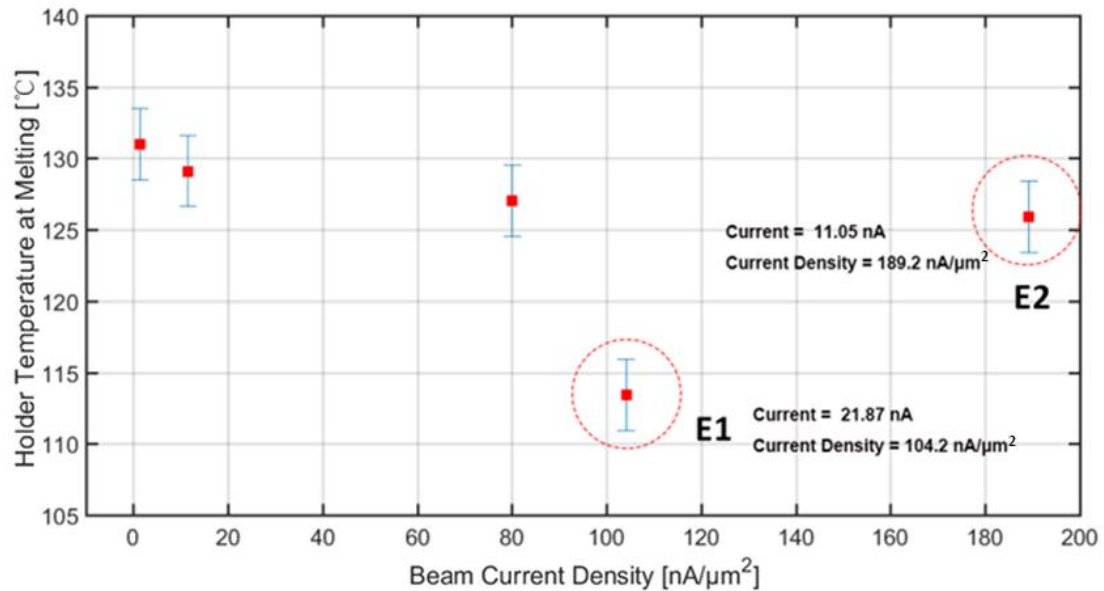


Figure 6.10: Holder temperature at melting point as a function of primary beam current density at 200 kV acceleration voltage. The island diameter is 100 nm.

In reference [5], the beam heating in an SEM is proposed to be proportional to the beam power. In our work, the beam heating in TEM shows a similar effect, see

Figure 6.11. A linear relationship between the beam heating and the beam power is found. As all data points from 120 kV and 200 kV show a good convergence in this linear plot, we propose that it is possible that the observed dependence on the acceleration voltage shown in Figure 6.9 is in fact a dependence on beam power. Figure 6.11 shows that the beam heating effect is lower than 5 °C at beam powers below 1000 μ W.

A size dependence of the beam heating is observed which is shown in Figure 6.12, Figure 6.13, and Figure 6.14. The electron beam heating effects of indium islands of 50 nm, 100 nm and 200 nm are shown in the different plots. It is clearly observable that for the *in situ* experiment at 120 kV, the electron beam heating is greater for smaller indium island. However, there is no observable dependence on the indium island size of the beam heating at 200 kV.

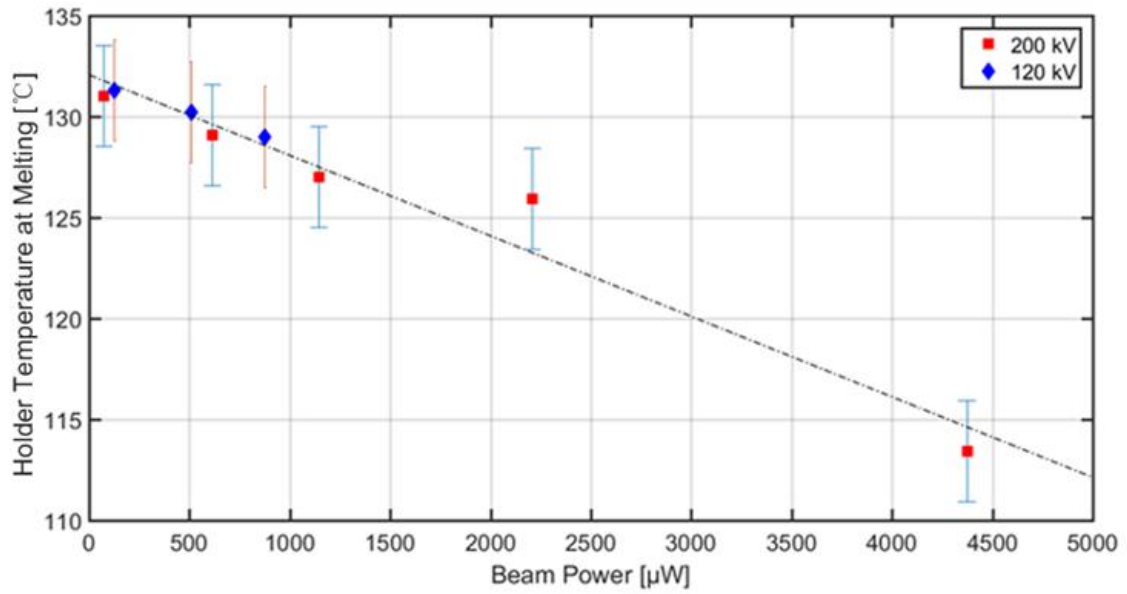


Figure 6.11: Holder temperature at melting point as a function of primary beam power. The island diameter is 100 nm. A linear relationship is found between the beam heating and the electron beam power.

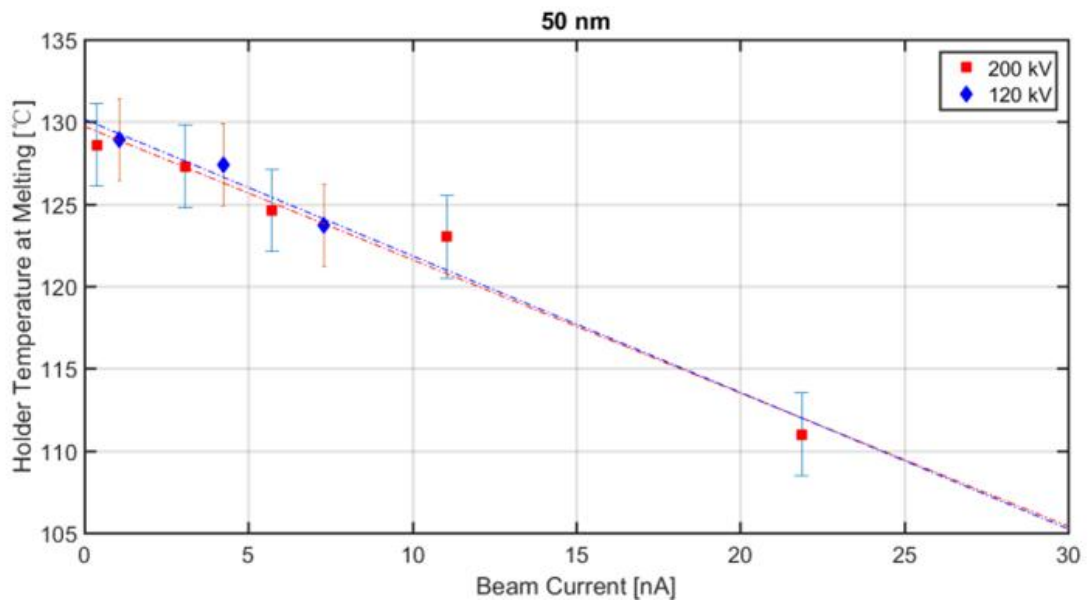


Figure 6.12: Holder temperature at melting point as a function of primary beam current. The island diameter is 50 nm.

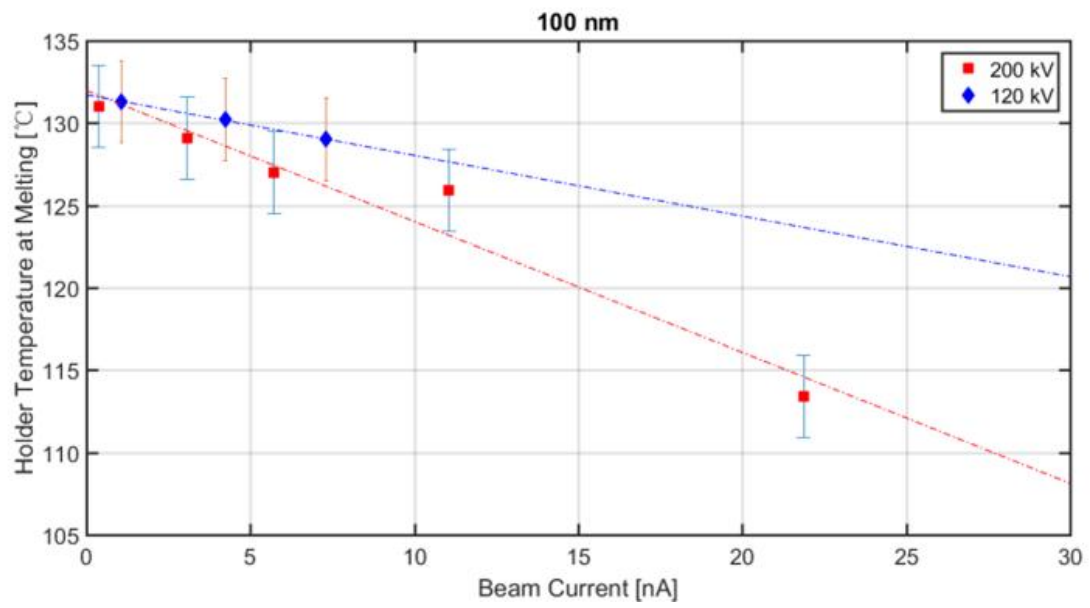


Figure 6.13: Holder temperature at melting point as a function of primary beam current. The island diameter is 100 nm.

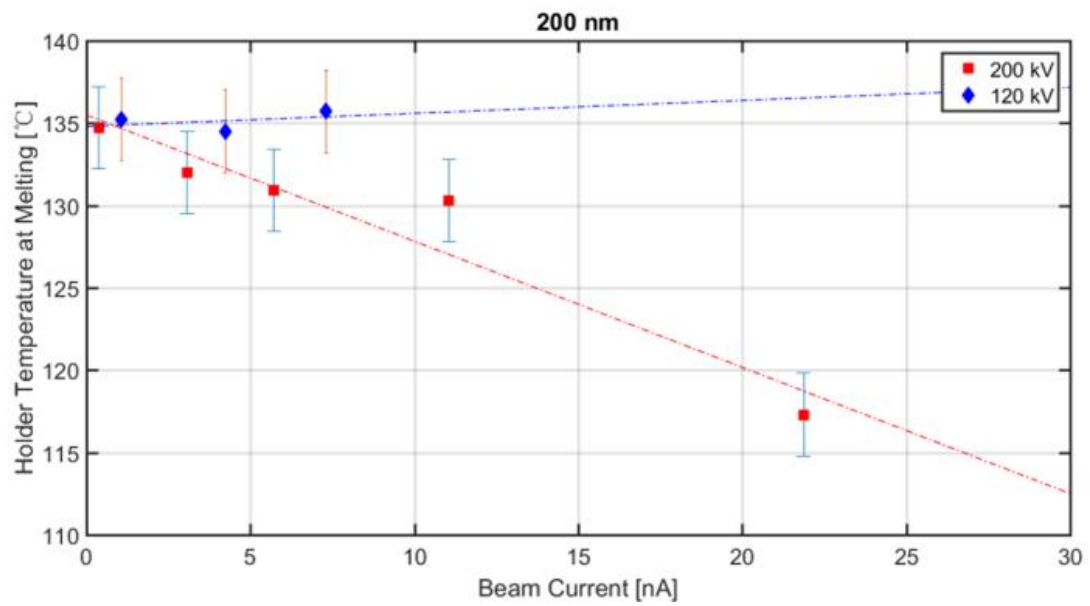


Figure 6.14: Holder temperature at melting as a function of primary beam current. The island diameter is 200 nm.

7

Conclusion & Future Plan

Electron beam heating can be significant and thus influence the data evaluation of *in situ* heating TEM results. The goal of this master thesis project is to develop an experimental approach to quantify the TEM electron beam heating.

In our project, *in situ* TEM heating experiments with different beam settings are performed on multiple nanoscale indium islands. A TEM heating holder is used to heat the samples. The relative beam heating is estimated from the change of holder temperatures recorded at the melting point of indium islands. The solid to liquid phase transition of indium island is identified through centered dark field imaging. Image processing including OTSU thresholding, watershed segmentation and image alignment is applied to identify and localize the indium islands.

To calibrate the electron beam current, a method to fabricate a homemade Faraday cup is developed in this work. First, a sharp gold tip is made by electrochemical etching where one-step and two-step etching recipes are compared. The Faraday cup is made by FIB using ion milling and platinum deposition. The gold tip with the Faraday cup is mounted in a *Nanofactory* instrument holder connected to a picoammeter that measures the beam current.

From our experiments, the electron beam heating is found to be proportional to the beam current. Nevertheless the size of the illumination area has no observable effect on the specimen heating. However, the effect of acceleration voltage on the beam heating is obvious. It is also shown that the beam heating is proportional to the primary beam power. An island size dependence on the beam heating is observed. In addition, at 120 kV acceleration voltage, the beam heating is greater for smaller islands while 200 kV gives no observable dependence on the indium island size of the beam heating.

In future work, it is of interest to improve the accuracy of the temperature control. This can be achieved by an advanced MEMS (Microelectromechanical Systems) heating holder. In order to understand the size and acceleration voltage dependence on the beam heating, additional experiments at intermediate acceleration voltages are needed.

A

Matlab Code

The MATLAB files for analysis of TEM images are listed here where functions as image reading, alignment, segmentation, island analysis and melting analysis are encoded.

A.1 Main File

The main file contains all of the function processes including firstly image reading then following image alignment indium island segmentation, islands analysis and melting analysis.

```
1 %% Project: A thermal in situ TEM study of indium nano islands.
2 % Author: Ren Qiu
3 % Course: Master thesis, TIF X61
4 % Main: image reading, Image alignment, OTSU thresholding, watershed segmentation,
5 % Island analysis, Melting Analysis, Image display.
6
7 clear all;
8 % Clear all data
9 clc;
10 % Clear display in command window
11
12 %% Image reading:
13 folder = 'E:\Master thesis\ Images of heating experiment';
14 files = dir([folder '\*.tif ']);
15 for i=1:numel(files)
16     imageName=strcat(num2str(i),'.tif');
17     I_transfer = imread(imageName);
18     I_transfer = double(rgb2gray(I_transfer));
19     % Transfer the unit 8 images into intensity image
20     I_transfer = (I_transfer -min(min(I_transfer)))*(1-0)/(max(max(I_transfer))...
21     -min(min(I_transfer)))+0;
22     % Normalization of the double image
23     I(:, :, i) = I_transfer;
24     % Transfer the temporary image into the image double matrix
25 end
26 T = [60 60 70 80 90 100 105 110 115 120 125 130 135 140 145 150 155 160 165 170 175...
27 180 160 140 120 100 80 60];
28 % Heating temperature sequence/image correspondence
29
30 %% Segmentation by OTSU and Watershed algorithms:
31 I_BF = I_aligned_cut(:, :, 1);
```

```

32 % Give the birght field image
33 [I_BF_OTSU, I_BF_OTSU_opening, I_BF_OTSU_filling, Threshold_BF, ...
34 I_BF_Watershed, I_BF_Watershed_noborder, I_BF_Watershed_gray] ...
35 = Segmentation(I_BF);
36 % Call the segmentation function for OTSU thresholding and Watershed segmentation
37 % I_BF_OTSU: binary image obtained from OTSU thresholding
38 % I_BF_OTSU_opening: morphological opening operation on I_BF_OTSU
39 % I_BF_OTSU_filling: holes filling on I_BF_OTSU_opening
40 % Threshold_BF: Optimal threshold from OTSU
41 % I_BF_Watershed: Segmentated image from Watershed segmentation
42 % I_BF_Watershed_noborder: Segmentated image without island edges
43 % I_BF_Watershed_gray: Segmentated image with island edge pixels in gray scale
44
45 %% Island Analysis:
46 [Island_property, Num_island] = Island_analysis(I_BF_Watershed);
47 % Island_property(n,1): Size estimated by the number of pixels of island "n"
48 % Island_property(n,2): Characteristic diameter of island "n" in nm
49 % Island_property(n,3): row-coordinate of center of island "n"
50 % Island_property(n,4): column-coordinate of center of island "n"
51
52 %% Melting Island Tracking:
53 [Island_Intensity, Island_Intensity_normalized, Island_Intensity_normalized_sub, ...
54 T_m_idx, Island_property] = Melting_islands_tracking(Island_property, ...
55 Num_island, I_BF_Watershed, I_aligned_cut, files);
56 % Call the island tracking function
57 % Island_Intensity: Averaged island intensity of all islands
58 % Island_Intensity_normalized: normalized intensity of islands
59 % Island_Intensity_normalized_sub: difference of island intensities
60 % T_m_idx: melting temperature sequence index
61
62 %% Showing the melting sequence:
63 T_start = 8;
64 T_end = 12;
65 [I_melt_set, I_melt] = ...
66 Melted_Island_Showing(T_start, T_end, Island_property, I_BF_Watershed);
67 % Call the melting analysis function
68 % I_melt_set: Islands melting sequences
69 % I_melt: all melted islands detected by the algorithm
70 image_display(I_melt_set)
71 % Show the island melting sequence
72 I_melt_normalized = ...
73 (I_melt - min(min(I_melt)))*(1-0)/(max(max(I_melt))-min(min(I_melt)))+0;
74 % Normalization of the melted islands image
75
76 %% Island melting data analysis:
77 [Area_melt_ratio, Mean_size, T_melt_idx, err, , Melting_temp] = ...
78 Melting_data(T_start, T_end, Island_property, I_BF_Watershed, files, Num_island)
79 % T_melt_idx: melting temperature index region manually input
80 % Area_melt_ratio: 2D Melting Area at each melting temperature
81 % Mean_size: Melted islands mean size at each temperature
82 % err: Standard deviation of melted island sizes at each temperature
83 %% Plot the Melting Temperature v.s. Island Size curve
84
85 %% Melting temperature:
86 [Melting_temp] = Melting_data_2(Island_property);
87 % Melting_temp is calculated to show the melting temperature of...

```

```
88 % indium island with specific island size
```

A.2 Image Alignment

This function is used for alignment of dark field images with respect to the bright field image where a selection of bright features in the dark field images should be done manually.

```
1 function I_aligned = Image_align(I, files)
2 % This function is used to align the dark field images with respect ...
3 % to the bright field image by rigid alignment without image warping
4 % I: image set to be aligned
5 % files: collection of images
6 % I_aligned: output image set after alignment
7
8 align_feature = zeros(2,numel(files));
9 % Define the image aligning feature variable for all images
10 figure(2)
11 % Display the reference image and target image to be aligned
12 for i = 1:numel(files)
13 % Find the image alignment feature location manually
14     subplot(1, 3, 1)
15     imshow(I(:, :, 1))
16     title('Bright Field Image')
17     subplot(1, 3, 2)
18     imshow(I(:, :, 2))
19     title('First Dark Field Image')
20     subplot(1, 3, 3)
21     imshow(I(:, :, i))
22     title('Image to be Aligned')
23     % Input the location of image alignment feature manually
24     align_feature(1, i) = input('Input the x-coordinate(right) of Feature for ...
25     Image Alignment: x = ');
26     align_feature(2, i) = input('Input the y-coordinate(down) of Feature for...
27     Image Alignment: y = ');
28     clc;
29 end
30
31 I_shift = zeros(2,numel(files));
32 for i = 1:numel(files)
33     I_shift(1, i) = align_feature(1, 1) - align_feature(1,i);
34     I_shift(2, i) = align_feature(2, 1) - align_feature(2, i);
35     I_aligned(:, :, i) = imtranslate(I(:, :, i), [I_shift(1, i), I_shift(2, i)]);
36     % Call the image translate function
37 end
38 end
39 % End of the function
```

A.3 Image Segmentation

This function gives the islands positions by OTSU thresholding following the Watershed segmentation.

```

1 function [I_BF_OTSU, I_BF_OTSU_opening, I_BF_OTSU_filling, ...
2 Threshold_BF, I_BF_Watershed, I_BF_Watershed_noborder, ...
3 I_BF_Watershed_gray] = Segmentation(I_BF)
4 % This function is used to segment the indium islands from the bright field image
5 % I_BF_OTSU: binary image obtained from OTSU thresholding
6 % I_BF_OTSU_opening: morphological opening operation on I_BF_OTSU
7 % I_BF_OTSU_filling: holes filling operation on I_BF_OTSU_opening
8 % Threshold_BF: Optimal threshold from OTSU
9 % I_BF_Watershed: Segmented image from Watershed segmentation
10 % I_BF_Watershed_noborder: Segmented image without island edges
11 % I_BF_Watershed_gray: Segmented image with island edge pixels in gray scale
12 % I_BF: input bright field image
13
14 Threshold_BF = graythresh(I_BF);
15 % Optimal threshold for segmentation by OSTU algorithm
16 I_BF_OTSU = im2bw(I_BF,Threshold_BF);
17 I_BF_OTSU = ~I_BF_OTSU + 1;
18 % Invert the pixel intensity between background and object
19 se = strel('disk', 1);
20 % Create a disc-like operation element for morphological operation
21 I_BF_OTSU_opening = imopen(I_BF_OTSU, se);
22 % Remove the tiny star object by Morphological Operation opening
23 I_BF_OTSU_filling = imfill(I_BF_OTSU_opening, 'holes');
24 % Filling the holes within the particles
25
26 %% Do the segmentation by Watershed algorithm:
27 Dis_tran = -bwdist(~I_BF_OTSU_filling);
28 Dis_tran_1 = Dis_tran;
29 Dis_tran(~I_BF_OTSU_filling) = -Inf;
30 Dis_tran_2 = Dis_tran;
31 I_transfer = imhmin(Dis_tran, 0.6);
32 % 0.6 is the height threshold for suppressing shallow minima avoiding over segmentation
33 I_BF_Watershed = watershed(I_transfer);
34 I_BF_Watershed_border = I_BF_Watershed ~= 1;
35 I_BF_Watershed_noborder = I_BF_Watershed > 1;
36
37 %% Convert the image for island edge display:
38 for i = 1:length(I_BF_OTSU)
39     for j = 1:length(I_BF_OTSU)
40         if I_BF_Watershed(i, j) == 0
41             I_BF_Watershed_gray(i, j) = 0.5;
42             % Border pixels defined to be 0.5 in gray scale image
43         elseif I_BF_Watershed(i, j) == 1
44             I_BF_Watershed_gray(i, j) = 0;
45             % Background pixels defined to be 0 in gray scale image
46         else
47             I_BF_Watershed_gray(i, j) = 1;
48             % Island pixels defined to be 1 in gray scale image
49         end

```

```

50     end
51 end
52
53 end
54 % End of the function

```

A.4 Island Analysis

This function is called for the island analysis where a size distribution histogram of indium islands and island centers are determined. Different probability distribution functions regarding the island size are evaluated by least square approach.

```

1 function [Island_property, Num_island] = Island_analysis(I_BF_Watershed)
2 % This function is used to do island size statistic analysis on "I_BF_Watershed"
3 % Island_property: matrix for important island properties
4 % Num_island: number of island obtained from the I_BF_Watershed
5 % I_BF_Watershed: binary image obtained from Watershed segmentation
6
7 Num_island = max(max(I_BF_Watershed));
8 Island_property = zeros(Num_island, 6);
9 % Define the Island_property matrix
10 for n = 2:Num_island
11 % Loop starts from n=2, get rid off the background
12     for i = 1:length(I_BF_Watershed)
13         for j = 1:length(I_BF_Watershed)
14             if I_BF_Watershed(i, j) == n
15                 Island_property(n, 1) = Island_property(n, 1) + 1;
16                 % Island size estimated by the number of pixels
17             end
18         end
19     end
20 end
21
22 Pixel_size = 200/25;
23 % Pixel size determination from the image scale bar manually
24 Island_property(:, 2) = sqrt(4*Island_property(:, 1)/pi) * Pixel_size;
25 % Island_property(:, 2): characteristic diameter in nm
26
27 %% Center of each Island determined from the pixel value average:
28 x_sum = 0;
29 y_sum = 0;
30 k = 0;
31 for n = 2:Num_island
32 % Start from n = 2, get rid off the background
33     for i = 1:length(I_BF_Watershed)
34         for j = 1:length(I_BF_Watershed)
35             if I_BF_Watershed(i, j) == n
36                 % If the pixel(i, j) belongs to island "n"
37                 x_sum = x_sum + i;
38                 y_sum = y_sum + j;
39                 k = k + 1;
40             end

```

```

41     end
42 end
43 Island_property(n, 3) = round(double(x_sum/k));
44 % Island_property(n, 3): row-coordinate of center of island "n"
45 Island_property(n,4) = round(double(y_sum/k));
46 % Island_property(n, 4): column-coordinate of center of island "n"
47 k = 0;
48 x_sum = 0;
49 y_sum = 0;
50 end
51
52 %% Differential particle size distribution function
53 Size_max = max(Island_property(:,2));
54 % Island size in nm
55 Bin_size = 10;
56 % Size of the histogram bins in nm
57 Bin_num = round(Size_max/Bin_size);
58 % Number of bins in the histogram
59 Hist = zeros(Bin_num, 1);
60 % Array for histogram bin value
61 Island_size_array = [];
62 % Island size array for histogram display
63 for i = 1:Bin_num
64 % Loop for finding island size histogram
65     for n = 2:Num_island
66         if Bin_size * (i-1) <= Island_property(n, 2) && ...
67             Island_property(n, 2) < i * Bin_size
68             % Divide the histogram into bins with size as "Bin_size"
69             Hist(i) = Hist(i) + 1;
70         end
71     end
72     Hist_frac(i) = double(Hist(i))/double(Num_island);
73     % Calculate the fraction of island size histogram
74     Island_size_array(i) = Bin_size/2 + (i-1) * Bin_size;
75     % Create an array for histogram bins
76 end
77 Island_size_fit = Island_size_array(1):1:Island_size_array(end);
78 % Create the x-axis array for the island size distribution function fitting
79
80 %% Normal Distribution
81 Norm_dist = fitdist(Island_property(2:Num_island, 2), 'normal');
82 Norm_fit = pdf(Norm_dist, Island_size_fit) * Bin_size;
83
84 %% Log-normal Distribution
85 Lognorm_dist = fitdist(Island_property(2:Num_island, 2), 'Lognormal');
86 Lognorm_fit = pdf(Lognorm_dist, Island_size_fit) * Bin_size;
87
88 %% Weibull Distribution
89 paramEsts = wblfit(Island_property(2:Num_island, 2));
90 Weibull_fit = wblpdf(Island_size_fit, paramEsts(1), paramEsts(2)) * Bin_size;
91
92 %% Gamma Distribution
93 Gamma_dist = fitdist(Island_property(2:Num_island, 2), 'gamma');
94 Gamma_fit = pdf(Gamma_dist, Island_size_fit) * Bin_size;
95
96 %% Plot Island Size Distribution

```

```

97 figure (1)
98 bar(Island_size_array, Hist_frac)
99 hold on;
100 grid on;
101 title ('Island Size Distribution')
102 set(gca, 'fontsize', 18, 'linewidth', 2)
103 xlabel('Island Size [nm]', 'fontsize', 18)
104 ylabel('Number Fraction', 'fontsize', 18)
105 plot(Island_size_array, Hist_frac, 'k o-', 'linewidth', 2)
106 plot(Island_size_fit, Lognorm_fit, 'm--', 'LineWidth', 2)
107 plot(Island_size_fit, Norm_fit, 'y--', 'LineWidth', 2)
108 plot(Island_size_fit, Gamma_fit, 'c--', 'LineWidth', 2)
109 plot(Island_size_fit, Weibull_fit, 'r--', 'linewidth', 2)
110 legend('Fractional histogram', 'Discrete distribution', 'Lognormal distribution', ...
111 'Normal distribution', 'Gamma distribution', 'Weibull distribution')
112
113 %% Least square validation of distribution functions:
114 ls_sum_norm = 0;
115 ls_sum_lognorm = 0;
116 ls_sum_weibull = 0;
117 ls_sum_gamma = 0;
118 % Initiate the error square summation of different probability distribution functions
119 for i = 1:Bin_num
120     ls_sum_norm = ls_sum_norm + ...
121         (Hist_frac(i) - Norm_fit(find(Island_size_fit == Island_size_array(i))))^2
122     % Summation of error square for normal distribution
123     % Function "find" output the correpondance between ...
124     % "Island_size_array" and the fitting distribution
125     ls_sum_lognorm = ls_sum_lognorm + ..
126         (Hist_frac(i) - Lognorm_fit(find(Island_size_fit == Island_size_array(i))))^2
127     % Summation of error square for lognormal distribution
128     ls_sum_gamma = ls_sum_gamma + ...
129         (Hist_frac(i) - Gamma_fit(find(Island_size_fit == Island_size_array(i))))^2
130     % Summation of error square for Gamma distribution
131     ls_sum_weibull = ls_sum_weibull + ...
132         (Hist_frac(i) - Weibull_fit(find(Island_size_fit == Island_size_array(i))))^2
133     % Summation of error square for Weibull distribution
134 end
135
136 end
137 % end of the function

```

A.5 Melting Analysis

This function is used to analyze the melting temperature of indium islands according to dark field images at each heating temperature based on the island segmentation and image alignment.

```

1 function [Island_Intensity, Island_Intensity_normalized, ...
2 Island_Intensity_normalized_sub, T_m_idx, Island_property] = Melting_islands_tracking ...
3 (Island_property, Num_island, I_BF_Watershed, I_aligned_cut, files)
4 %% This function is used to analyze the melting process to find out ...

```

```

5 %% the melting temperature of each island
6 % Island_Intensity: pixel intensity variation of each island
7 % Island_Intensity_normalized: average pixel intensity variation of each island
8 % Island_Intensity_normalized_sub: difference of average pixel intensity ...
9 % variation of each island
10 % T_m_idx: melting temperature sequence index
11 % Island_property: matrix for important island properties
12 % Num_island: number of island obtained from the I_BF_Watershed
13 % I_BF_Watershed: binary image obtained from Watershed segmentation
14
15 I_aligned_cut_label = I_aligned_cut;
16 % Create a new image set for function operation
17
18 %% Calculate the sum of intensity for each island in each temperature:
19 Island_Intensity = zeros(Num_island,numel(files));
20 for k =2:numel(files)
21 % Image sequence/temperature "k" starts from "2" as the first image is the bright field image
22     for n = 2:Num_island
23         % Island sequence, starts from "2" as the background is "1"
24         for i = 1:length(I_aligned_cut)
25             for j = 1:length(I_aligned_cut)
26                 if I_BF_Watershed(i, j) == n
27                     Island_Intensity(n, k) = Island_Intensity(n, k) ...
28                         + I_aligned_cut(i, j, k);
29                     % Summation of pixel values in one island
30                 end
31             end
32         end
33     end
34 end
35
36 %% Average the island intensity summation:
37 for k = 2:numel(files)
38 % Image sequence/temperature "k" starts from "2" as the first image is the bright field image
39     for n = 2:Num_island
40         % Island sequence, starts from "2" as the background is "1"
41         Island_Intensity_normalized(n, k) = Island_Intensity(n, k)/Island_property(n, 1);
42         Island_Intensity_normalized_sub(n, k) = Island_Intensity_normalized(n, k) ...
43             - Island_Intensity_normalized(n, k-1);
44         % Intensity Differential Variation
45     end
46 end
47
48 figure(1)
49 % Check the melting island melting process
50 for n = 1:Num_island
51     if Island_property(n, 1) > 30 & n ~= 132
52         % Threshold out the small islands with pixel number <= 30, ...
53         % compensate for the mislignment
54         plot(Island_Intensity_normalized(n, 1:numel(files)), 'o-')
55         % plot(Island_Intensity_normalized_sub(n, 1:numel(files)), 'o-')
56         hold on;
57     end
58 end
59 axis([2 28 -0.1 0.6])
60 % axis([3 20 -0.2 0.3])

```

```

61 xlabel('Temperature sequence', 'fontsize', 18)
62 ylabel('Normalized intensity ', 'fontsize', 18)
63 % ylabel('Normalized intensity difference ', 'fontsize', 18)
64 grid on;
65 set(gca, 'fontsize', 18, 'linewidth', 2)
66
67 %% Find the Melting Temperature for each Island:
68 T_start = 6;
69 T_end = 13;
70 % Define a rough melting regime manually
71 for n = 2:Num_island
72     [a b] = max(Island_Intensity_normalized_sub(n, T_start:T_end));
73     if a >= 0.095 & Island_property(n, 1) > 30
74         % Only count the island containing more than 30 pixels
75         Island_property(n, 5) = b + T_start - 1;
76         % Index of the melting temperature of island n
77     else
78         Island_property(n, 5) = -1;
79         % Does not fit the melting threshold condition
80     end
81 end
82
83 %% Refine the code for temperature correlation:
84 Tm_idx = [60 70 80 90 100 105 110 115 120 125 130 135 140 145 150];
85 for n = 2:Num_island
86     if T_m_idx(n) == -1
87         Island_property(n, 6) = 0;
88         % Unmelted island or undetected islands
89     else
90         Island_property(n, 6) = Tm_idx(T_m_idx(n));
91         % Melting temperature of each island correlated
92     end
93 end
94
95 end
96 % End of the function

```

A.6 Melting Sequence Analysis

This function is called for classification of indium islands according to their melting temperature following the melting analysis function.

```

1 function [I_melt_set, I_melt] = Melted_Island_Showing ...
2 (T_start, T_end, Island_property, I_BF_Watershed)
3 %% This function is used to divide the indium islands into groups ...
4 %% according to their melting temperature
5 % I_melt_set: image set of island with different melting temperatures
6 % I_melt: all islands detected to be melted
7 % T_start: the first melting happens
8 % T_end: the last melting happens
9 % Island_property: matrix for important island properties
10 % I_BF_Watershed: binary image obtained from Watershed segmentation
11

```

```

12 I_melt_set = zeros(length(I_BF_Watershed), ...
13 length(I_BF_Watershed), T_end-T_start+1);
14 % Create the image set for island melting sequence
15 I_melt = zeros(length(I_BF_Watershed), length(I_BF_Watershed));
16 % Create the matrix for all melted islands
17 for k = 1 : (T_end - T_start + 1)
18     for i = 1 : length(I_BF_Watershed)
19         for j = 1 : length(I_BF_Watershed)
20             if I_BF_Watershed(i, j) >= 2
21                 if Island_property(I_BF_Watershed(i, j), 5) == (k + T_start - 1);
22                     I_melt_set(i, j, k) = k;
23                 end
24             end
25         end
26     end
27 end
28 I_melt = I_melt + I_melt_set(:, :, k);
29 end
30
31 end
32 % End of the function

```

A.7 Melting Data

The functions are called to calculate the data of melting of the interested indium islands.

```

1 function [Area_melt_ratio, Mean_size, T_melt_idx, err, Melting_temp] = Melting_data(
2     T_start, T_end, Island_property, I_BF_Watershed, files, Num_island)
3 % This function is to calculate the data from the melting experiment for plotting
4 %% Define the matrix and array to be needed:
5 Island_size_idx = [];
6 Area_melt = zeros(numel(files),1);
7 Area_sum = 0;
8 %% Count the islands sizes and melted area size at each temperature
9 Area_sum = 0;
10 for i = T_start:1:T_end
11     j = 1;
12     for n = 2:Num_island
13         if Island_property(n,5) == i % i = 8 9 10 11 12
14             Island_size_idx(i,j) = Island_property(n,2); % Characteristic Diameter
15             Area_melt(i) = Area_melt(i) + Island_property(n,1); % Number of pixels
16             j=j+1;
17         end
18     end
19     Area_sum = Area_sum + Area_melt(i);
20 end
21 %% Creat data for plotting
22 for i = T_start:1:T_end
23     a = [];
24     a = Island_size_idx(i,:);
25     a(a==0)=[];
26     [mu(i),sigma(i)] = normfit(a);

```

```

26 end
27
28 Mean_size = mu(T_start:T_end);
29 err = sigma(T_start:T_end);
30 T_melt_idx = T_start:1:T_end;
31 Area_melt_ratio = Area_melt/Area_sum;
32
33 for i = 2:length(Area_melt_ratio)
34     Area_melt_ratio(i) = Area_melt_ratio(i) + Area_melt_ratio(i-1);
35 end
36
37 Area_melt_ratio = Area_melt_ratio(T_start:T_end);
38
39 Size_max = max(Island_property(:,3));
40 Bin_size = 8;
41 Bin_num = round(Size_max/Bin_size);
42 Melt_temp = zeros(Bin_num,2);
43 for i = 1:Bin_num
44     Temp_transfer = [];
45     for n = 2:Num_island
46         if Bin_size*(i-1) <= Island_property(n,2) && Island_property(n,2) < i*Bin_size &&
47             Island_property(n,5) > 0
48             Temp_transfer = [Temp_transfer Island_property(n,5)];
49         end
50     end
51     Melt_temp(i,1) = mean(Temp_transfer);           % Melting temperature average
52     Melt_temp(i,2) = std(Temp_transfer);           % Error bar for melting temperature
53     Melt_temp(i,3) = (2*i-1)/2*Bin_size;          % Middle point of the bin
54 end
55 Melt_temp_1 = [];
56 Melt_temp_2 = [];
57 Melt_temp_3 = [];
58 for i = 1:Bin_num
59     if Melt_temp(i,1) >= 0 && Melt_temp(i,3) >= 25
60         Melt_temp_1 = [Melt_temp_1 Melt_temp(i,1)];
61         Melt_temp_2 = [Melt_temp_2 Melt_temp(i,2)];
62         Melt_temp_3 = [Melt_temp_3 Melt_temp(i,3)];
63     end
64 end
65 clear Melt_temp;
66 Melt_temp(:,1) = Melt_temp_1;                     % Melting temperatures
67 Melt_temp(:,2) = Melt_temp_2;                     % Error bars of the melting temperatures
68 Melt_temp(:,3) = Melt_temp_3;                     % Middle points of all islands diameters
69 Melt_temp(:,4) = double(1./Melt_temp(:,3));       % Inverse of the islands diameters
70
71 %% Plot the Melting Area Ratio v.s. Melting Temperatures
72 % Linear regression: y=p(1)*x+p(2)
73 p = polyfit(Melt_temp(:,4),Melt_temp(:,1),1)
74 xx = 0:0.0001:0.040;
75 yy = p(1) * xx + p(2);
76 plot(Melt_temp(:,4),Melt_temp(:,1),'s','linewidth', 2);
77 % errorbar(Melt_temp(:,4),Melt_temp(:,1),Melt_temp(:,2),'s r','linewidth', 2)
78 hold on;
79 plot(xx,yy,'r','linewidth', 2)
80 % axis([0 0.02 108 122])
81 xlabel('1/Diameter [1/nm]','fontsize',18)

```

A. MATLAB Code

```

81 ylabel('Melting Temperature [ $130^{\circ}\mathrm{C}$ ]', 'fontsize', 18)
82 grid on;
83 set(gca, 'fontsize', 18, 'linewidth', 2)
84 % legend('')
85 end
86 % end of the function

```

```

1 function [Melting_temp] = Melting_data_2(Island_property)
2 %% Melting_temp is the array containing melting temperature of island of interested size
3 Size_max = max(Island_property(:,3));
4 Bin_size = 8;
5 Bin_num = round(Size_max/Bin_size);
6 Melt_temp = zeros(Bin_num,2);
7 for i = 1:Bin_num
8     Temp_transfer = [];
9     for n = 2:Num_island
10        if Bin_size*(i-1) <= Island_property(n,2) && Island_property(n,2) < i*Bin_size &&
11           Island_property(n,6) >0
12           Temp_transfer = [Temp_transfer Island_property(n,6)];
13           % Melting temperature of one specific island size of each Bin
14        end
15    end
16    Melt_temp(i,1) = mean(Temp_transfer);
17    % Melting temperature average – this term is the one that shall be changed !!!!!!!!!!!
18    Melt_temp(i,2) = std(Temp_transfer);
19    % Error bar for melting temperature
20    Melt_temp(i,3) = (2*i-1)/2*Bin_size;
21    % Middle point of the bin
22 %% Refinement with consideration of the confidential interval of 95%:
23    Upper_limit = Melt_temp(i,1) + 1.96 * Melt_temp(i,2);
24    Lower_limit = Melt_temp(i,1) - 1.96 * Melt_temp(i,2);
25    Tm_sum = 0;
26    num = 0;
27    for n = 2:Num_island
28        if Bin_size*(i-1) <= Island_property(n,2) && Island_property(n,2) < i*Bin_size &&
29           Island_property(n,6) >0
30           if Island_property(n,6) >= Lower_limit && Island_property(n,6) <= Upper_limit
31               Tm_sum = Tm_sum + Island_property(n,6);
32               num = num+1;
33           end
34        end
35    end
36    Melt_temp(i,1) = Tm_sum/num;
37 end
38 Melt_temp_1 = [];
39 Melt_temp_2 = [];
40 Melt_temp_3 = [];
41 for i = 1:Bin_num
42     if Melt_temp(i,1) >=0 && Melt_temp(i,3) >=0
43         Melt_temp_1 = [Melt_temp_1 Melt_temp(i,1)];
44         Melt_temp_2 = [Melt_temp_2 Melt_temp(i,2)];
45         Melt_temp_3 = [Melt_temp_3 Melt_temp(i,3)];
46     end
47 end
48 clear Melt_temp;

```

```

48 Melt_temp(:,1) = Melt_temp_1;           % Melting temperatures
49 Melt_temp(:,2) = Melt_temp_2;         % Error bars of the melting temperatures
50 Melt_temp(:,3) = Melt_temp_3;         % Middle points of all islands diameters
51 Melt_temp(:,4) = double(1./Melt_temp(:,3)); % Inverse of the islands diameters
52 plot(Melt_temp(:,4), Melt_temp(:,1), 'o')
53 Inverse_island_size = Melt_temp(:,4)
54 Melting_Temperature = Melt_temp(:,1)
55 end
56 % end of the function

```

A.8 Image Display

This function is used for displaying image set in an order. Clicking on any button on the keyboard clicked is to go forward and clicking the mouse is to go backwards in the image sequence.

```

1 function image_display(I)
2 %% This function is used to display image set
3 %% Author: Kokchun Giang
4 % I: image set you want to display
5 % Operation: click any button to go forward; click mouse to go backwards
6
7 i = 0;
8 size_I=size(I);
9 colormap gray
10 while true
11     k = waitforbuttonpress;
12     if k == 1
13         i = i + 1
14     else
15         i = i - 1
16     end
17
18     if i >= 1 && i <= size_I(3);
19         imagesc(I(:, :, i));
20         axis equal
21     else
22         disp('The slice does not exist');
23         disp('The function is over.')
24         return;
25     end
26 end
27
28 end
29 % End of the function

```


Bibliography

- [1] R. F. Egerton, P. Li, M. Malac. Radiation damage in the TEM and SEM. *Micron*, 35: 399–409, 2004.
- [2] D. B. Williams, and C. B. Carter. Transmission electron microscopy - A textbook for materials science. *Springer Science and Business Media*, 2009.
- [3] R. F. Egerton. Control of radiation damage in the TEM. *Ultramicroscopy*, 127: 100-108, 2013.
- [4] N. Jiang, J. C. H. Spence. On the dose-rate threshold of beam damage in TEM. *Ultramicroscopy*, 113: 77-82, 2012.
- [5] D. Bouscaud, R. Pesci, S. Berveiller, E. Patoor. Estimation of the electron beam-induced specimen heating and the emitted X-rays spatial resolution by Kossel microdiffraction in a scanning electron microscope. *Ultramicroscopy*, 115: 115-119, 2012.
- [6] J. J. Hren, and J. I. Goldstein, D. C. Joy. Introduction to analytical electron microscopy. *Springer Science and Business Media*, 1979.
- [7] T. Brintlinger, Y. Qi, K. H. Baloch, D. Goldhaber-Gordon, and J. Cumings. Electron thermal microscopy. *Nano Letters*, 8: 582–585, 2008.
- [8] K. H. Baloch, N. Voskanian, M. Bronsgeest and J. Cumings. Remote Joule heating by a carbon nanotube. *Nature Nanotechnology*, 7: 316–319, 2012.
- [9] Retrived May 2017, from: https://en.wikipedia.org/wiki/Transmission_electron_microscopy
- [10] Retrived March 2017, from: https://en.wikipedia.org/wiki/Silicon_nitride
- [11] Retrived March 2017, from: <http://www.norcada.com/products/nitride-windows-tem/>
- [12] Retrived March 2017, from: <https://en.wikipedia.org/wiki/Indium>

- [13] B. Ren, G. Picardi and B. Pettinger. Preparation of gold tips suitable for tip-enhanced Raman spectroscopy and light emission by electrochemical etching. *Review of Scientific Instruments*, 75: 837–841, 2004.
- [14] M. Lopes, T. Toury , M. Lamy, L. Chapelle, F. Bonaccorso , P. G. Gucciardi. Image segmentation: A watershed transformation algorithm. *Image Anal Stereol*, 84: 73702-1–73702-8, 2013.
- [15] G. Xu, Z. Liu, K. Xu, Y. Zhang, H. Zhong, Y. Fan, and Z. Huang. Constant current etching of gold tips suitable for tip-enhanced Raman spectroscopy. *Review of Scientific Instruments*, 83: 103708-1–103708-5, 2012.
- [16] L. Eligal, F. Culfaz, V. McCaughan, N. I. Cade, and D. Richards. Etching gold tips suitable for tip-enhanced near-field optical microscopy. *Review of Scientific Instruments*, 80: 033701-1–033701-3, 2009.
- [17] L. Billot, L. Berguiga, M.L. de la Chapellea, Y. Gilbert, and R. Bachelot. Production of gold tips for tip-enhanced near-field optical microscopy and spectroscopy: analysis of the etching parameters. *The European Physical Journal Applied Physics*, 31: 139–145, 2005.
- [18] C. Williams and D. Roy. Fabrication of gold tips suitable for tip-enhanced Raman spectroscopy. *Journal of Vacuum Science & Technology B*, 26: 1761–1764, 2008.
- [19] D. Roy, C. M. Williams and K. Mingard. Single-crystal gold tip for tip-enhanced Raman spectroscopy. *Journal of Vacuum Science & Technology B*, 28: 631–634, 2010.
- [20] D. Gingery and P. Bühlmann. Single-step electrochemical method for producing very sharp Au scanning tunneling microscopy tips. *Review of Scientific Instruments*, 78: 113703-1–085105-4, 2007.
- [21] X. Wang, Z. Liu, M. Zhuang, H. Zhang, X. Wang, Z. Xie, D. Wu, B. Ren, and Z. Tian. Tip-enhanced Raman spectroscopy for investigating adsorbed species on a single-crystal surface using electrochemically prepared Au tips. *Applied Physics Letters*, 91: 101105-1–101105-3, 2007.
- [22] J. Parka, T.S. Hong, N.S. Lee, K.B. Kim, Yongho Seo. Viscosity dependence of electrochemical etching for gold tip fabrication. *Current Applied Physics*, 11: 1332–1336, 2011.
- [23] S. Narasiwodeyar. Two-step fabrication technique of gold tips for use in point-contact spectroscopy. *Review of Scientific Instruments*, 86: 033903-1–033903-5, 2015.

-
- [24] B.W. Mao, B. Ren, X.W. Cai and L.H. Xiong. Electrochemical oscillatory behavior under a scanning electrochemical microscopic configuration. *Journal of Electroanalytical Chemistry*, 394: 155–160, 1995.
- [25] J. Goldstein, D. Newbury, P. Echlin, D. Joy, C. Lyman, E. Lifshin, L. Sawyer, and J. Michael. *Scanning Electron Microscopy and X-Ray Microanalysis*. Springer Science and Business Media, 2003.
- [26] Retrived April 2017, from: <http://www.agarscientific.com/fr/tem/grids-agar.html>
- [27] N. Otsu. A threshold selection method from gray-level histograms. *IEEE Transactions on Systems, Man, and Cybernetics*, SMC-9: 62–66, 1979.
- [28] S. Beucher, and C. Lantuejoul. Use of watershed in contour detection. *International Workshop on Image Processing: Real-time Edge and Motion Detection/Estimation*, 2.1–2.12, 1979.
- [29] L. J. Belaid, and W. Mourou. Image segmentation: A watershed transformation algorithm. *Image Anal Stereol*, 28: 93–102, 2009.
- [30] Retrived April 2017, from: <https://se.mathworks.com/company/newsletters/articles/the-watershed-transform-strategies-for-image-segmentation.html>
- [31] C. Albonetti, M. Cavallini, M. Massi, and J. F. Moulin. Electrochemical preparation of cobalt tips for scanning tunneling microscopy. *Review of Scientific Instruments*, 73: 4254–4256, 2002.
- [32] M. Cavallini and F. Biscarini. Electrochemically etched nickel tips for spin polarized scanning tunneling microscopy. *Review of Scientific Instruments*, 71: 4457–4460, 2000.
- [33] L. Meng, T. Huang, X. Wang, S. Chen, Z. Yang, and B. Ren. Gold-coated AFM tips for tip-enhanced Raman spectroscopy: theoretical calculation and experimental demonstration. *Optics Express*, 23: 13804–138313, 2015.
- [34] T. Ishida, K. Kakushima, N. Sasaki, and H. Fujita. In situ TEM observation of nanobonding formation between silicon MEMS tips. *Nanotechnology*, 21: 435705-1–435705-5, 2010.
- [35] M. Meisnar, M. Moody, S. Lozano-Perez. Atom probe tomography of stress corrosion crack tips in SUS316 stainless steels. *Corrosion Science*, 98: 661–671, 2015.
- [36] R. D. Piner, J. Zhu, F. Xu, S. Hong, and C. A. Mirkin. "Dip-Pen" Nanolithography. *Science*, 283: 661–663, 1999.

- [37] D. S. Ginger, H. Zhang, C. A. Mirkin. The Evolution of Dip-Pen Nanolithography. *Angewandte Chemie (International ed.)*, 43: 30–45, 2004.
- [38] N. Mausera and A. Hartschuh. Tip-Enhanced Near-Field Optical Microscopy. *Angewandte Chemie (International ed.)*, 47: 8187–8191, 2008.